



# **1 The extremely hot and dry 2018 summer in central and 2 northern Europe from a multi-faceted weather and climate 3 perspective**

4 Efi Rousi<sup>1</sup>, Andreas H. Fink<sup>2</sup>, Lauren S. Andersen<sup>1</sup>, Florian N. Becker<sup>2</sup>, Goratz Beobide-  
 5 Arsuaga<sup>3,4</sup>, Marcus Breil<sup>2,5</sup>, Giacomo Cozzi<sup>6,7</sup>, Jens Heinke<sup>1</sup>, Lisa Jach<sup>8</sup>, Deborah Niermann<sup>9</sup>,  
 6 Dragan Petrovic<sup>10</sup>, Andy Richling<sup>11</sup>, Johannes Riebold<sup>12</sup>, Stella Steidl<sup>9</sup>, Laura Suarez-  
 7 Gutierrez<sup>13</sup>, Jordis Tradowsky<sup>6,14</sup>, Dim Coumou<sup>1,15,16</sup>, André Düsterhus<sup>17</sup>, Florian Ellsäßer<sup>18</sup>,  
 8 Georgios Fragkoulidis<sup>19</sup>, Daniel Gliksman<sup>20,21</sup>, Dörthe Handorf<sup>12</sup>, Karsten Haustein<sup>22,#</sup>, Kai  
 9 Kornhuber<sup>1,23,24</sup>, Harald Kunstmann<sup>7,10</sup>, Joaquim G. Pinto<sup>2</sup>, Kirsten Warrach-Sagi<sup>8</sup>, Elena  
 10 Xoplaki<sup>18,25</sup>

11 <sup>1</sup>Potsdam Institute of Climate Impact Research (PIK), Member of the Leibniz Association, Potsdam, Germany

12 <sup>2</sup>Institute of Meteorology and Climate Research (IMK-TRO), Karlsruhe Institute of Technology, Karlsruhe,  
 13 Germany

14 <sup>3</sup>International Max Planck Research School on Earth System Modelling (IMPRS-ESM), Germany

15 <sup>4</sup>Institute of Oceanography, Center for Earth System Sustainability, Hamburg University, Hamburg, Germany

16 <sup>5</sup>University of Hohenheim, Hohenheim, Germany

17 <sup>6</sup>Deutscher Wetterdienst, Regionales Klimabüro Potsdam, Stahnsdorf, Germany,

18 <sup>7</sup>University of Augsburg, Augsburg, Germany

19 <sup>8</sup>University of Hohenheim, Hohenheim, Germany

20 <sup>9</sup>Deutscher Wetterdienst, Offenbach, Germany

21 <sup>10</sup>Institute of Meteorology and Climate Research (IMK-IFU), Karlsruhe Institute of Technology, Campus Alpin,  
 22 Garmisch-Partenkirchen, Germany

23 <sup>11</sup>Institute of Meteorology, Free University of Berlin, Berlin, Germany

24 <sup>12</sup>Alfred Wegener Institute, Helmholtz Centre for Polar and Marine Research, Potsdam, Germany

25 <sup>13</sup>Max-Planck-Institut für Meteorologie, Hamburg, Germany

26 <sup>14</sup>Bodeker Scientific, Alexandra, New Zealand

27 <sup>15</sup>IVM-Institute for Environmental Studies, Free University of Amsterdam, Amsterdam, Netherlands

28 <sup>16</sup>Royal Netherlands Meteorological Institute (KNMI), De Bilt, Netherlands

29 <sup>17</sup>Irish Climate Analysis and Research UnitS (ICARUS), Department of Geography, Maynooth University,  
 30 Maynooth, Ireland

31 <sup>18</sup>Centre of International Development and Environmental Research, Justus Liebig University Giessen, Giessen,  
 32 Germany

33 <sup>19</sup>Institute for Atmospheric Physics, Johannes Gutenberg University, Mainz, Germany

34 <sup>20</sup>Institute for Hydrology and Meteorology, Faculty of Environmental Sciences, Technische Universität  
 35 Dresden, Tharandt, Germany

36 <sup>21</sup>Institute of Geography, Technische Universität Dresden, Dresden, Germany



37 <sup>22</sup>Climate Service Center Germany (GERICS), Helmholtz-Zentrum hereon, Hamburg, Germany

38 <sup>23</sup>Lamont-Doherty Earth observatory, Columbia University, New York, US

39 <sup>24</sup>German Council on Foreign Relations, Berlin, Germany

40 <sup>25</sup>Institute of Geography, Justus Liebig University Giessen, Giessen, Germany

41 # Now at Institute for Meteorology, University of Leipzig, Leipzig, Germany

42 *Correspondence to:* Efi Rousi ([rousi@pik-potsdam.de](mailto:rousi@pik-potsdam.de)) and Andreas H. Fink ([andreas.fink@kit.edu](mailto:andreas.fink@kit.edu))

43 **Abstract.** The summer of 2018 was an extraordinary season in climatological terms for northern and  
 44 central Europe, bringing simultaneous, widespread, and concurrent heat and drought extremes in large  
 45 parts of the continent with extensive impacts on agriculture, forests, water supply, and socio-economic  
 46 sector. We present a comprehensive, multi-faceted analysis of the 2018 extreme summer in terms of  
 47 heat and drought in central and northern Europe with a particular focus on Germany. The heatwave first  
 48 affected Scandinavia by mid-July, shifted towards central Europe in late July, while Iberia was primarily  
 49 affected in early August. The atmospheric circulation was characterized by strongly positive blocking  
 50 anomalies over Europe, in combination with a positive summer North Atlantic Oscillation and a double  
 51 jet stream configuration before the initiation of the heatwave. In terms of possible precursors common  
 52 to previous European heatwaves, the Eurasian double jet structure and a tripolar sea-surface temperature  
 53 anomaly over the North Atlantic were identified already in spring. While in the early stages over  
 54 Scandinavia the air masses at mid- and upper-levels were often of remote, maritime origin, at later  
 55 stages over Iberia the air masses had primarily a local to regional origin. The drought affected Germany  
 56 the most, starting with warmer than average conditions in spring, associated with enhanced latent heat  
 57 release that initiated a severe depletion of soil moisture. During summer, a continued precipitation  
 58 deficit exacerbated the problem, leading to hydrological and agricultural drought. A probabilistic  
 59 attribution assessment of the heatwave in Germany showed that the prolonged heat has become more  
 60 likely due to global warming. Regarding future projections, an extreme summer such as this of 2018 is  
 61 expected to occur every two out of three years in Europe under a 1.5 °C warmer world and virtually  
 62 every single year under 2 °C of global warming. With such large-scale and impactful extreme events  
 63 becoming more frequent and intense under anthropogenic climate change, comprehensive and multi-  
 64 faceted studies like the one presented here quantify the multitude of effects and provide valuable  
 65 information as basis for adaptation and mitigation strategies.

## 66 1 Introduction

67 Following an anomalously warm and dry spring, the summer of 2018 was characterized by record  
 68 breaking widespread heat and drought across Europe (Kennedy et al., 2019; Toreti et al., 2019) with  
 69 intense heatwaves affecting large parts of Scandinavia (Sinclair et al., 2019) and central Europe (e.g.,



70 Vogel et al. 2019). In Germany, both the months of April-May, as well as the April-July period, and the  
 71 entire year, were identified as the warmest in the observational records starting in 1881. Moreover,  
 72 Germany faced remarkably prolonged drought from February to November, with 2018 being the fourth  
 73 driest year on record (after 1959, 1911, and 1921). A new record was also set for annual sunshine  
 74 duration, amounting to 2015 hours (Friedrich and Kaspar, 2019). In Finland, the peak temperature in  
 75 summer exceeded 33 °C, which is extremely unusual for a region located near the Arctic Circle,  
 76 breaking historical records of the past 40 years (Liu et al., 2020). In the UK, summer 2018 joined 2006  
 77 as the hottest on record since 1884. In England itself, this was the warmest on record, while June 2018  
 78 was the driest June for England since 1925 (Kendon et al., 2019). Over the Iberian peninsula, a heatwave  
 79 developed in early August 2018, with this month being the warmest in the region after 2003  
 80 (Barriopedro et al., 2020). The normal eastward propagation of weather systems was hindered in  
 81 summer 2018 by the recurrent presence of blocking anticyclones, associated with a particularly  
 82 meandering jet stream, which was reflected in the way the heatwave propagated, starting in Scandinavia  
 83 (peaking mid of July), then developing in central Europe (end of July) and last in Iberia (beginning of  
 84 August). For the European continent, 2018 was the second warmest summer on record (following 2010)  
 85 as estimated from the CRUTEM4 dataset (Kennedy et al., 2019), prior to being marginally surpassed  
 86 by the 2021 summer (Copernicus Climate Change Service, 2018; 2021).

87 In terms of amplitude, persistence and spatial extent, the 2018 heatwaves were comparable to the  
 88 “mega-heatwaves” of 2003 and 2010 over Europe and Russia (Spensberger et al., 2020; Becker et al.,  
 89 2022), during which more than one million square kilometers were simultaneously affected by heatwave  
 90 conditions (Fink et al., 2004; Barriopedro et al., 2011). But, unlike 2003 and 2010, the exceptionally  
 91 extreme heat in 2018 occurred under concurrent exceptionally dry conditions, thus making the events  
 92 in 2018 a spatially and temporally compound extreme (Zscheischler et al. 2020; Bastos et al. 2021;  
 93 Ionita et al., 2021). These co-occurring hot and dry extremes, not only in central Europe but also in  
 94 multiple regions of the northern hemisphere midlatitudes (Vogel et al., 2019), caused vast aggregated  
 95 impacts (Bakke et al., 2020), ranging from drought-inflicted forest mortality events of unprecedented  
 96 scale (Schuldt et al., 2020; Senf and Seidl, 2021), up to 50 % reduction in agricultural yields (Toreti et  
 97 al., 2019; Beillouin et al., 2020) and increased forest fire occurrence (San-Miguel-Ayaz et al., 2019),  
 98 to excess heat-related human mortality (Pascal et al., 2021). Compared to previous droughts since 2000,  
 99 summer 2018 occupied the largest extent of extreme and severe agriculture drought, centered around  
 100 Germany, Poland, most of Scandinavia and the Baltic countries, affecting a larger extent of boreal  
 101 forests and high latitude ecosystems (Peters et al., 2020). Further, from a temporal point of view,  
 102 compared to other droughts of the past 40 years, 2018 was characterized by the sharpest transition from  
 103 average-to-wet conditions in late winter to extremely strong soil-water deficits in summer (Bastos et  
 104 al., 2020).

105 Surface heatwaves are typically co-located with the center of the associated blocking system (Kautz  
 106 et al., 2022; their Figure 2b). If the blocking is intense and persistent, a heatwave will usually develop.



On the other hand, unsteady weather conditions, like thunderstorms and heavy precipitation, are frequent on the flanks of the blocking system, which correspond to the air mass boundaries (Kautz et al., 2022). In fact, summer extremes can be exacerbated by different components of the Earth system, such as anomalous atmospheric circulation patterns, oceanic conditions, and the state of land surface (Wehrli et al., 2019; Di Capua et al., 2021). The atmospheric circulation during late spring and summer 2018 was characterized by the frequent presence of atmospheric blocking, and a persistent positive summer North Atlantic Oscillation (sNAO; Drouard et al., 2019; Li et al., 2020). Among the possible precursors of European heatwaves, here we analyzed spring sea-surface temperatures (SST) over the North Atlantic and soil moisture anomalies over Europe. In particular, the tripolar North Atlantic SST anomaly pattern is known to be influenced by the winter NAO, persisting over spring and affecting European climate in summer (Herceg-Bulić and Kucharski, 2014). The North Atlantic tripolar pattern has been associated with the East Atlantic Pattern (Gastineau and Frankignoul, 2015) and Atlantic Ridges (Ossó et al., 2020), leading to decreased summer precipitation (Saeed et al., 2013; Rousi et al., 2021) and increased summer temperatures over Europe (Chen et al., 2016). Additionally, Duchez et al. (2016) argues that a cold anomaly over the North Atlantic subpolar gyre (SPG) may be associated with a stationary position of the jet stream, enhancing European summer heat extremes. Moreover, soil moisture-temperature feedbacks can amplify heat extremes (Seneviratne et al., 2010). Through a positive feedback, soil moisture depletion by hot and dry atmospheric conditions leads to a reduction of evaporative cooling and suppressed convective available potential energy (CAPE) values, subsequently limiting the rainfall potential and increasing air temperatures further (Miralles et al., 2014; Prodhomme et al., 2021).

Hot and dry summers in Europe are expected to occur more frequently under anthropogenic global warming (Masson-Delmotte et al. IPCC, 2021). McCarthy et al. (2019) conducted an attribution study for the 2018 summer heatwave in the UK based on CMIP5 models and found that the present-day likelihood of such extremes is around 11 %, which has been made 30-times higher due to anthropogenic climate change, while this likelihood increases to 53 % by the 2050s. Given the increase of hot and dry extremes in Europe (Manning et al., 2019; Perkins-Kirkpatrick and Lewis, 2020; Markonis et al., 2021) and their further expected increase under continued unmitigated anthropogenic climate change (Russo et al., 2014; 2015; Spinoni et al., 2018; 2020), comprehensive weather and climate studies analyzing regional heatwave and drought characteristics, drivers, and impacts are particularly important.

Within the German research initiative ClimXtreme, about 140 scientists from 35 institutions joined in 39 projects to further understand climate extremes, focusing on central Europe (<https://climxtreme.net/index.php/en/>). Inter-disciplinary task forces were formed, among which one on heat and drought. This study brings together its members to study the 2018 European heat and drought from a multi-faceted weather and climate perspective, making it the first comprehensive study looking at hot and dry summers over Europe using different analyses approaches to study (a) the extremeness and attribution to anthropogenic climate change (climate perspective), as well as (b) the synoptic



144 dynamics in concert with the role of slowly varying boundary conditions at the ocean and continental  
 145 surfaces (seasonal and weather perspective). In the following, first, the data and methods are presented  
 146 (Sect. 2). Different metrics for the detection and description of the 2018 summer extremes are shown  
 147 in Sect. 3.1. Then, we present various features of the atmospheric circulation including blocking, jet  
 148 stream state, weather regimes, Rossby wave activity and air mass trajectories (see Sect. 3.2). Next, the  
 149 role of low-frequency precursors, i.e. SSTs and soil moisture in spring, in setting the scene and  
 150 eventually shaping those extremes is investigated (see Sect. 3.3). Sect. 3.4. examines the event from a  
 151 large-ensemble climate model perspective, accompanied by a tailored attribution analysis of the  
 152 heatwave in Germany based on CMIP6 models. The Discussion and Conclusions section completes this  
 153 paper.

## 154 **2 Data and Methods**

### 155 **2.1 Data**

156 In this paper we use a variety of datasets, including observational, reanalysis and model data. We are  
 157 using a common spatial domain for Europe (10° W–50 °E, 30°-70° N) and the reference period 1981–  
 158 2010 unless otherwise stated.

159 ERA5 (Hersbach et al., 2020) and ERA5-HEAT (Di Napoli et al., 2021) reanalysis datasets were  
 160 utilized for the calculation of heatwave metrics (see Sect. 3.1), the dynamical drivers and their evolution,  
 161 such as Rossby wave activity, backward trajectories, double jet streams, atmospheric blocking, and  
 162 weather regimes (see Sect. 3.2), as well as the precursors, i.e. SSTs and soil moisture (see Sect. 3.3). E-  
 163 OBS gridded observational datasets (Haylock et al., 2008; Cornes et al., 2018) were used for the  
 164 calculation of the drought indices (SPI, SPEI), for the drought detection with climate networks (see  
 165 Sect. 3.1), and to estimate the return period of the heatwave and select equivalent extreme events in  
 166 CMIP6 model simulations for the attribution study (see Sect. 3.4). Observational datasets from DWD  
 167 stations (Kaspar et al., 2013) were used for the thermopluviogram for Germany (see Sect. 3.1).

168 The dynamic vegetation model „LPJmL5-tillage“ (Von Bloh et al., 2018; Schaphoff et al., 2018;  
 169 Lutz et al., 2019) was used to simulate soil moisture as forced by climate parameters (i.e. temperature,  
 170 precipitation, wind) from the GSWP3-W5E5 dataset, a combination of GSWP3 v1.09 (Kim, 2017) and  
 171 a bias-adjusted version of ERA5 reanalysis data (Lange, 2019). The simulation was run under evolving  
 172 CO<sub>2</sub> and pre-industrial natural vegetation conditions (see Sect 3.3).

173 The historical and RCP4.5 simulations of the Max Planck Grand Ensemble (MPI-GE; Maher et al.,  
 174 2019) were used to calculate the cumulative excess heat under recent climate (1979-2021), and future  
 175 1.5° C (2020-2049) and 2° C (2050-2079) warmer worlds (see Sect. 3.4). The advantage of this dataset  
 176 is that, apart from the forced response, it provides an estimate of the internal natural variability.  
 177 Historical simulations of several Coupled Model Intercomparison Project Phase 6 models (CMIP6;



178 Eyring et al., 2016) and pre-industrial type simulations (hist-nat) of the same models from the CMIP6-  
 179 endorsed Detection and Attribution Model Intercomparison Project (DAMIP; Gillett et al., 2016) were  
 180 used for the probabilistic attribution study (see Sect. 3.4). An overview of the analyzed CMIP6 models  
 181 is given in Table A1.

## 182 **2.2 Methods**

### 183 **2.2.1 Heatwave metrics**

184 Despite the fact that heatwaves have been a topic of active climate research for many decades, there is  
 185 no universal heatwave definition and there are multiple metrics and criteria depending on the region,  
 186 the season, and the purpose of the study (Becker et al., 2022). Here, we chose two different metrics to  
 187 characterize heatwave intensity, the cumulative heat, which uses temperature only, and the cumulative  
 188 Universal Thermal Climate Index (cUTCI) that represents human thermal comfort, taking into account  
 189 temperature, humidity, wind, and radiation.

190 A heatwave was defined here as an event of at least three consecutive days during which the 90<sup>th</sup>  
 191 percentile of the daily maximum temperature based on each calendar day is exceeded (Fischer and  
 192 Schär, 2010). Cumulative heat refers to the integration of heat exceedance over the threshold for all  
 193 heatwave days of a season. In the present study, only summer months (June to August; JJA) were  
 194 considered, hence combining the intensity and persistence of heatwaves (Perkins-Kirkpatrick and  
 195 Lewis, 2020). The cUTCI was calculated for each day as in Błazejczyk et al. (2013) and the 90<sup>th</sup>  
 196 percentile of the daily time series was defined. The cumulative intensity was then calculated as the  
 197 integration of the exceedance above this threshold for the whole season.

### 198 **2.2.2 Drought indicators**

199 For the characterization and detection of the 2018 drought we used two widely accepted indicators, the  
 200 Standardized Precipitation Index (SPI; McKee et al., 1993) and the Standardized Precipitation  
 201 Evapotranspiration Index (SPEI; Vicente-Serrano et al., 2014), and one alternative method based on  
 202 climate networks (Tsonis et al., 2006; Donges et al., 2009).

203 Two aggregation periods, three and six months, were selected, so that two types of droughts, could  
 204 be considered, meteorological (SPEI3) and agricultural (SPEI6) (Heim, 2002; Zampieri et al., 2017).  
 205 The SPEI was calculated with the SPEI R Package (Beguería and Vicente-Serrano, 2013). For the SPI,  
 206 monthly precipitation sums were used, while for the SPEI additionally monthly mean maximum and  
 207 minimum temperatures were needed for the calculation of the potential evapotranspiration (PET). This  
 208 was conducted based on the modified Hargreaves equation (Droogers and Allen, 2002). The method  
 209 corrects the PET calculated by the Hargreaves equation by using the monthly rainfall amount as a proxy  
 210 for insolation and based on the hypothesis that this amount can change the humidity levels (Vicente-



211 Serrano et al., 2014). The values obtained by this method are similar to those obtained from the Penman-  
 212 Monteith method (Allen et al., 2006).

213 Further, a climate network approach was used (Tsonis et al., 2006; Donges et al., 2009) to detect  
 214 drought conditions in Germany. In a climate network, high spatial coherence of weather conditions is  
 215 characterized by high values of the node degree measure that accounts for pairwise statistical similarity  
 216 (e.g. quantified with the Pearson correlation coefficient; for more details about the construction of the  
 217 climate network see Schädler and Breil, 2021). In this context, the node degree of a single grid point is  
 218 the number of network nodes (or grid points) connected to it. The higher the node degrees of a climate  
 219 network, the higher the spatial coherence of the meteorological time series and thus, the similarity of  
 220 the weather conditions. Since droughts are typically extensive and persistent events, high node degrees  
 221 can be used as a good drought indicator.

### 222 **2.2.3 Atmospheric circulation metrics**

223 The large-scale atmospheric circulation patterns and the dynamical evolution of the atmosphere  
 224 associated with the 2018 extremes were analyzed using various metrics. First, we looked at the weather  
 225 regimes during summer in order to characterize large-scale circulation features. Five summer  
 226 circulation regimes were computed with k-means clustering (Crasemann et al., 2017) applied to ERA5  
 227 sea-level pressure (SLP) anomalies for the time period 1979-2018 over the North Atlantic/European  
 228 region (30-88° N, 90° W - 90° E). Further, blocking frequency anomalies were calculated at a grid point  
 229 level based on a slightly modified version of the two-dimensional blocking index from Scherrer et al.  
 230 (2006). Daily blocked grid points were identified based on gradients in the daily 500 hPa geopotential  
 231 height (gph) field and on areas of positive gph anomalies associated with the blocking detection, as  
 232 described in Schuster et al. (2019).

233 Next, we looked at the state of the jet stream. Jet stream states were identified with the use of Self-  
 234 Organizing Maps (SOMs), a neural network-based clustering algorithm (Kohonen, 2013; Rousi et al.,  
 235 2015). SOMs were applied on daily ERA5 data of Eurasian (25-80° N, 25° W - 180° E) zonal-mean  
 236 zonal wind data on different pressure levels (800 hPa -100 hPa) for the time period 1979-2020 (see  
 237 details in Rousi et al., 2022). Moreover, we applied the methodology of Fragkoulidis and Wirth (2020)  
 238 to identify Rossby wave packets and their amplitude (E) for the 2018 summer. The method employs the  
 239 meridional wind field (v) at 300 hPa at 2x2 degree resolution, which was taken from the ERA5 data.  
 240 The visualization of E and v (see Fig. 4) is adaptive to the latitude location of strong Rossby wave  
 241 packets and only the latitudinal belt of 40-90° N was taken into account. For each longitude, E and v  
 242 are averaged over 10 grid points that exceed the median of all values within that belt.

243 To analyze the origin of the air masses during the 2018 summer heatwave, we calculated backward  
 244 trajectories using Lagrangian analysis and the LAGRANTO tool (Sprenger and Wernli, 2015). In  
 245 particular, we calculated 10-day backward trajectories for the levels between 1000 and 500 hPa in steps  
 246 of 25 hPa using ERA5 data for three starting locations in Europe on the respective peak heatwave days.





247 As in Zschenderlein et al. (2020), starting points were also taken within the upper-tropospheric blocking  
 248 anticyclone, in this case over Scandinavia. These were defined as the grid points where the anomaly of  
 249 the vertically averaged potential vorticity (between 500 and 150 hPa, based on monthly climatology)  
 250 was below  $-0.7$  PVU ( $1 \text{ PVU} = 10^{-6} \text{ K kg}^{-1} \text{ m}^2 \text{ s}^{-1}$ ). For all grid points that fulfilled this criterion,  
 251 trajectories were initialized every 50 hPa between 500 and 150 hPa in the vertical dimension. To exclude  
 252 starting points in the stratosphere, only grid points with  $PV < 1$  PVU were considered.

#### 253 **2.2.4 Low-frequency precursors**

254 In order to analyze low-frequency precursors of the summer 2018 extremes, we considered SSTs, total  
 255 precipitation and soil moisture in the preceding months. The SST anomalies, compared to the reference  
 256 period of 1981-2010, over the North Atlantic and the seas surrounding Europe (Mediterranean, North  
 257 Sea, Baltic Sea) were analyzed for the spring (March to May; MAM) and summer (June to August;  
 258 JJA) months of 2018 in ERA5 data. Precipitation and soil moisture anomalies over Europe were also  
 259 calculated for the same seasons in ERA5, and for soil moisture LPJmL simulations were also used.

260 Additionally, we derived time series for the soil moisture-latent heat flux correlation in Germany  
 261 based on ERA5 reanalysis data and LPJmL output with a daily temporal resolution based on centered  
 262 92-day running windows. This approach was used because soil moisture limitation depends on various  
 263 factors, such as the climatic conditions and vegetation characteristics (rooting depth, Leaf Area Index  
 264 (LAI) and stomatal conductance), which vary spatially and can change during the course of a year (Duan  
 265 et al., 2020). Therefore, the limitation cannot be easily represented by a unified, fixed value. The time  
 266 series were spatially averaged over all land points for Northern Germany and surroundings ( $51-55^\circ \text{ N}$   
 267 and  $4-16^\circ \text{ E}$ ), as well as southern Germany and surroundings ( $48-51^\circ \text{ N}$  and  $4-16^\circ \text{ E}$ ). The German  
 268 Alpine region was not included in the southern German region because the complex topography that  
 269 cannot be accounted for in this study, influences the results.

#### 270 **2.2.5 Attribution of the 2018 extreme heat**

271 Extreme event attribution typically addresses the question of whether and to what extent climate change  
 272 has affected the severity and/or frequency of a specific extreme weather event (Shepherd, 2016). The  
 273 most commonly used approach to extreme event attribution is probabilistic event attribution (Philip et  
 274 al., 2020), which compares climate model simulations under different scenarios, i.e. a factual scenario  
 275 which simulates the weather under current and past climate conditions, and a counterfactual scenario  
 276 which simulates weather under climate conditions excluding anthropogenic influences.

277 Here we present two kinds of attribution approaches. In the first, we used the MPI-GE to estimate  
 278 the probability of exceedance of the 2018 summer heat levels in the whole European domain for present  
 279 and future climates, and in the second, we present a tailored extreme event attribution study for  
 280 Germany based on CMIP6 simulations to calculate probability ratios for the persistent 2018 heat event  
 281 in Germany.





282 The MPI-GE (Maher et al., 2019) was used to estimate and compare the probabilities of exceeding  
 283 the 2018 summer levels of cumulative heat in the reanalysis data (ERA5, 1979–2021) and under recent  
 284 (1979–2021), and future 1.5° C (2020–2049) and 2° C (2050–2079) warmer worlds. The same heatwave  
 285 metric and parameters were used to calculate the cumulative heat as the ones described above (Sect.  
 286 2.2.1). The ERA5 data were regridded to a coarser resolution to match that of the MPI-GE and the  
 287 probabilities were normalized to percentages (i.e. divided by the total number of years in each period).

288 Then, to estimate how the occurrence probability of the 2018 heatwave in Germany has been affected  
 289 by anthropogenic climate change, a tailored probabilistic attribution study was conducted using CMIP6  
 290 simulations. The historical CMIP6 simulations provide the factual scenario while hist-nat simulations  
 291 from DAMIP provide the counterfactual scenario. The analysis is based on an attribution system  
 292 currently under development at DWD within the ClimXtreme project and involves (1) defining the  
 293 extreme event, (2) analyzing observational data and estimating the probability/return period of such an  
 294 event based on observations, (3) validating the climate model simulations, (4) preparing and analyzing  
 295 the climate model simulations, and (5) calculating a probability ratio between the historical and hist-nat  
 296 simulations.

297 Based on CMIP/DAMIP data available at the computing facility of the German Climate Computing  
 298 Center (DKRZ) the most appropriate climate models were selected for the tailored attribution study by  
 299 including the ones that had at least three initializations in the DAMIP archive and passed the validation  
 300 tests outlined below for the maximum temperature (Tmax) that is analyzed in the attribution study. The  
 301 climatology of Tmax and the spatial pattern of the yearly averaged maximum temperature were visually  
 302 compared between the models and the gridded E-OBS dataset to evaluate whether the models are able  
 303 to represent the climate conditions over Germany. Additionally, the parameters of a Generalized  
 304 Extreme Value (GEV) distribution fitted to the simulation data were compared with a fit to the E-OBS  
 305 data to check whether they agree within their uncertainty bounds. Furthermore, a general consistency  
 306 check was performed for each model ensemble. The evaluation procedure is similar to the one used in  
 307 World Weather Attribution studies (see e.g. Philip et al., 2020). Simulations of CMIP6 models that  
 308 passed the validation were further analyzed (see Table A1 for a list of the models).

309 The following steps are required to calculate the risk ratio: CMIP and DAMIP Tmax data from all  
 310 available initializations of the model were selected for the German region and for the 30-year timeframe  
 311 from 1985–2014. The data were averaged over the region and a 17-day running mean was calculated,  
 312 based on the event definition which is further elaborated in Sect. 3.4. The yearly block maxima were  
 313 then selected from all initializations and a GEV fit was used to estimate the probability of heatwaves in  
 314 the simulation data that are equivalent to the observed event of 2018. To account for offsets between  
 315 observed and simulated temperatures, we analyzed a simulated heat event which has – in the historical  
 316 simulations – the same probability as the observed heatwave, i.e. while the simulated event may not  
 317 reach the same temperature as was observed in 2018, the temperature threshold used to analyze the  
 318 simulations has the same return period as the observed event (see also Philip et al., 2020; Tradosky et



al., 2022). To increase the robustness of the results a 1000-member bootstrap was used and a GEV distribution was fitted to each of these 1000 alternative time series. The probability ratios (PR) were then calculated from the probabilities of such heatwaves in the historical and hist-nat simulations using the GEV fits to the original simulation time series and to the 1000 alternative time series, according to equation (1):

$$PR = \frac{P_{historical}}{P_{hist-nat}} \quad (1)$$

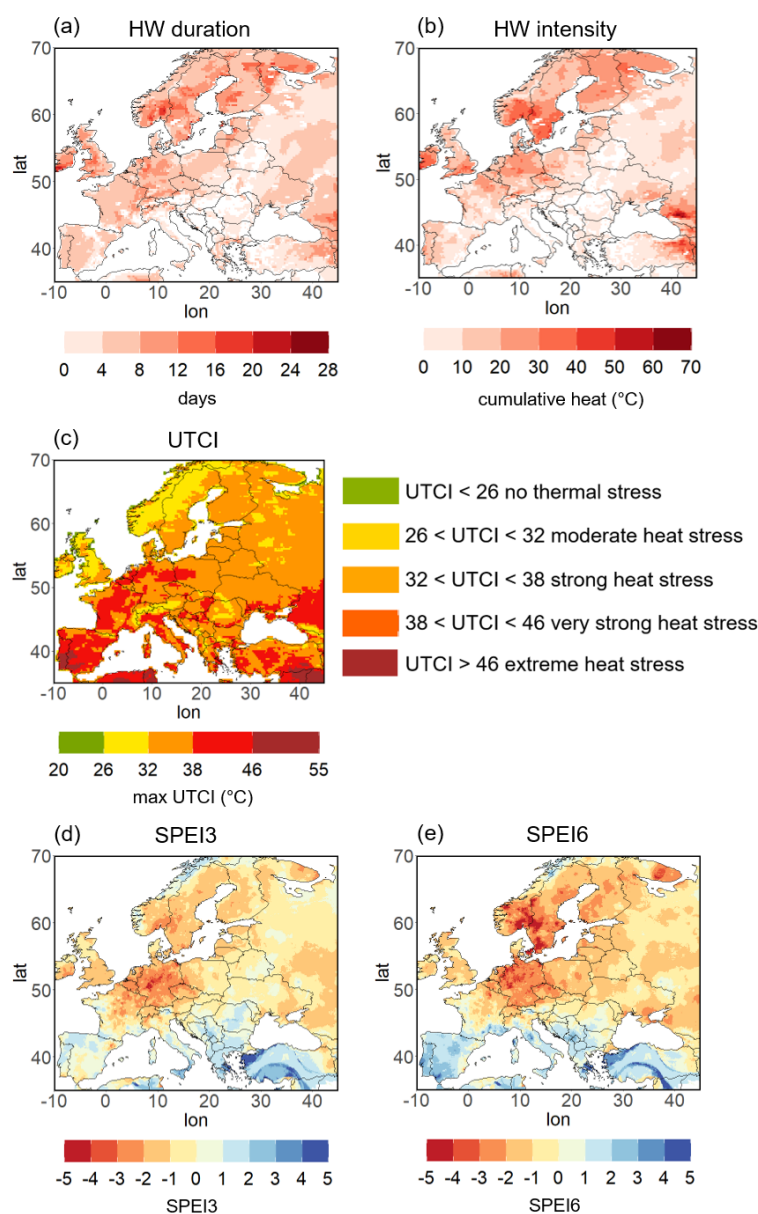
$P_{historical}$  is the probability of the event to occur in the historical CMIP scenario and  $P_{hist-nat}$  is the probability in the naturalized DAMIP scenario in which anthropogenic greenhouse gas emissions are fixed to pre-industrial times.

A probability ratio  $> 1$  indicates an increase in the probability of such an event due to anthropogenic climate change, a result which is typically found for recent heatwaves (see e.g. Stott et al., 2004; Philip et al., 2021).

### 3 Results

#### 3.1 Detection and description of the 2018 summer extremes

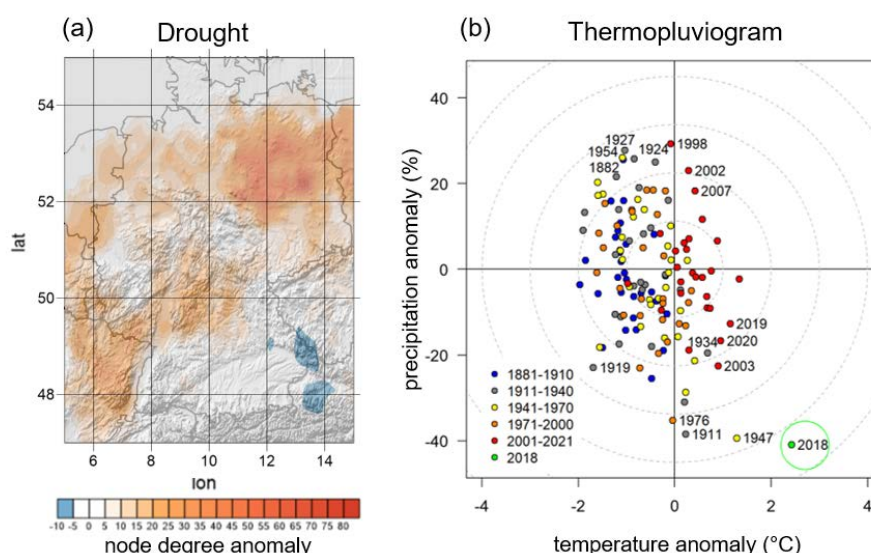
The 2018 summer was an extreme season from the climatological perspective for many regions in Europe. An intense heatwave first affected Scandinavia in mid-July and then extended towards central Europe and later Iberia, spanning a total period of four weeks. The maximum heatwave duration was seen in Scandinavian regions, reaching 20 consecutive days (Fig. 1a). Cumulative heat reached peak values in parts of Norway, Sweden, Germany, France, Ireland and the UK (Fig. 1b). The cUTCI index showed periods of extreme heat stress in Portugal and southwestern Spain, very strong heat stress in northern and central Germany, central-western Poland, large parts of France and Iberia, and strong heat stress in most of eastern Europe, Finland, southern Scandinavia and parts of the British Isles (Fig. 1c). The high intensities in Turkey and the Caucasian region were not caused by the same weather pattern as the event described in this paper and are thus not discussed here.



343  
 344 **Figure 1:** Spatial representation of European heatwave (ERA5) and drought (E-OBS) in the 2018  
 345 summer. (a) Maximum heatwave duration in days (grid point-based, exceedance of 90<sup>th</sup> percentile of  
 346 daily maximum temperature). (b) Cumulative heat (in °C). (c) Maximum UTCI in the 2018 summer per  
 347 grid point and respective heat stress category. (d) SPEI3 August. (e) SPEI6 August. Respective maps  
 348 for SPI can be found in the Appendix (Fig. A1). Reference period used in all metrics: 1981-2010.



349 In northern and central Europe, the heatwave was preceded and accompanied by intense drought  
 350 conditions. As an example, the meteorological drought is depicted in terms of the SPEI3 and SPEI6  
 351 values for August (Fig. 1d,e) that were particularly low in central and northern Europe (correspondent  
 352 SPI shown in Fig. A1). The cumulative effect of low precipitation and high evapotranspiration lead to  
 353 lower values of the SPEI6 index in many European regions compared to SPEI3. The most extreme  
 354 values ( $\text{SPEI6} < -5$ ) are identified for southern Norway and Sweden. For Germany, the drought  
 355 conditions can also be seen when using the complementary approach based on climate networks  
 356 (Schädler and Breil, 2021). Figure 2a shows the spatial distribution of node degree anomalies, compared  
 357 to the reference period 1981-2010, for dry days in Germany for the 2018 summer, as a measure of  
 358 drought spatial coherence (connectivity). High anomaly values are identified for large areas in central  
 359 and northern Germany highlighting the exceptional drought, while no anomalies are found over south  
 360 Germany. The thermopluviogram for Germany depicts temperature and precipitation anomalies for  
 361 Germany, and confirms that the extended warm period of April to October 2018 was the most  
 362 exceptional in terms of precipitation deficit and heat anomaly compared to the reference period (1981-  
 363 2010) since 1881 (Fig. 2b). When considering different seasonal periods, such as March to August, or  
 364 June to August only, 2018 remains a very extreme season (see Fig. A2). In summary, while the heatwave  
 365 was most intense in southern Scandinavia, 2018 stood out as the most intense compound heat and dry  
 366 event in the observational history for Germany, in agreement with Zscheischler and Fischer (2020).



367  
 368 **Figure 2:** Summer 2018 heatwave and drought in Germany. (a) Climate network node degree anomaly  
 369 (as a proxy for spatial coherence) for dry days in summer (June to August; JJA) 2018 in Germany (E-  
 370 OBS data, reference period 1981-2010). (b) Thermopluviogram for the growing season, April to



371 October, of the years 1881-2021 for Germany showing the temperature and precipitation anomalies  
 372 from the climatological mean (DWD observational data, reference period 1981-2010). 2018 is  
 373 highlighted with light green color. Thermopluviograms for different periods can be found in the  
 374 Appendix (Fig. A2).

### 375 **3.2 Dynamical drivers and evolution**

376 In order to characterize large-scale circulation features for summer 2018, we used a number of different  
 377 and complementary metrics to describe the multi-faceted characteristics of the event. First, we analyzed  
 378 the blocking conditions for this season, as the occurrence of heatwaves is directly associated with  
 379 summer blocking or – for the lower latitudes in Europe – to atmospheric ridges (Woollings et al., 2018;  
 380 Sousa et al., 2018; Kautz et al., 2022). Using the blocking detection algorithm, we confirm that for the  
 381 2018 summer, blocking is detected over Great Britain from late June into the first ten days of July as  
 382 well as over Scandinavian and Ural regions for most days of July (Fig. A3). Compared to the  
 383 climatological occurrence of blocking frequency, the percentage of blocked days in June/July 2018 was  
 384 20-60 % higher in the mentioned areas (Fig. 3a,b), indicating blocking frequency values above the 90<sup>th</sup>  
 385 percentile (Fig. A4). This large-scale set up for the summer time (see e.g., Kautz et al., 2022, their  
 386 Figure 2b) leads to the development of a heatwave collocated with the center of the blocking, while  
 387 unsteady weather conditions may happen on the block edges.

388 The establishment of a long-lived blocking anticyclone is consistent with the development of a  
 389 double jet stream state over Eurasia, with two maxima of the zonal mean zonal wind at the 250 hPa  
 390 level, which started as early as mid-May and persisted until 25<sup>th</sup> of July, with only a few days in between  
 391 not characterized by double jets (Fig. 3c). The period 04–25 July was characterized by a continuous  
 392 persistent double jet configuration, according to the SOM-based detection scheme of jet stream states.  
 393 These 22 consecutive days of double jets make 2018 one of the longest such events in the study period  
 394 (1979–2020), the longest being that of 2003 (Rousi et al., 2022; their Figure 4). The initiation of the  
 395 heatwave in Europe happened a few days after the initiation of this persistent double jet event (see Fig.  
 396 4), highlighting a potential role of the double jet structure in preconditioning the flow and favoring the  
 397 onset of a heatwave in the region of weak winds between the two jets, where the blocking anticyclone  
 398 lies (Rousi et al., 2022). This large-scale set up typically corresponds to the occurrence of the summer  
 399 NAO+ (sNAO+) regime, as confirmed by the circulation regime approach applied on the 2018 summer.  
 400 Indeed, most of July 2018 was dominated by a sNAO+ pattern, typically characterized by a more  
 401 northerly location and smaller spatial scale than its winter counterpart (Folland et al., 2009). This is in  
 402 agreement with previous studies (e.g. Drouard et al., 2019) showing a strong positive EOF-based NAO  
 403 anomaly in this time period that is consistent with large parts of the seasonal anomalies observed during  
 404 summer 2018.

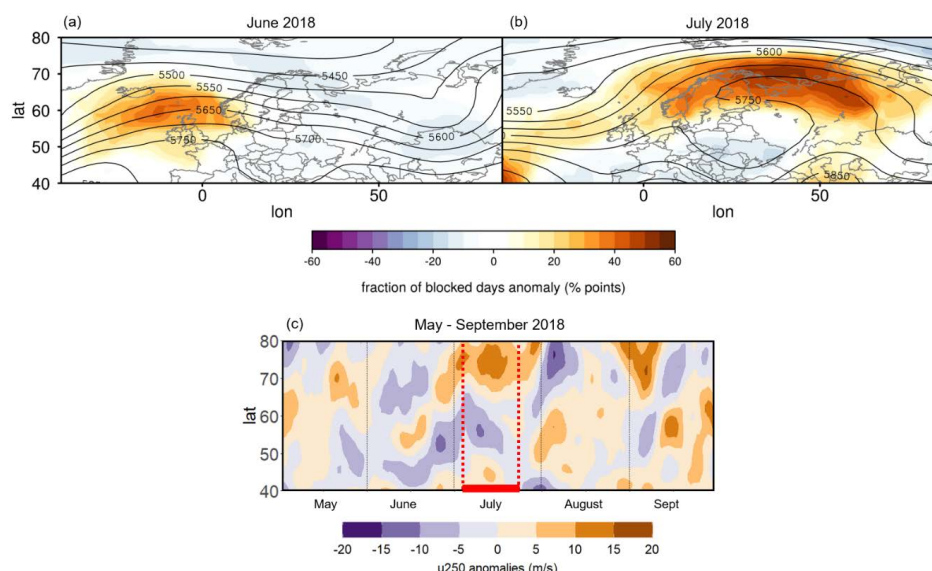


**Figure 3:** Blocking frequency anomalies for (a) June and (b) July 2018 (shading, contour lines show mean geopotential height at 500hPa plotted every 50hPa). (c) Eurasian zonal mean zonal wind at 250hPa for May-September 2018 (shading; 5day running means centered on each day from 01.05-30.09.2018). The red lines mark the duration of the longest double jet event (04-25.07.2018).

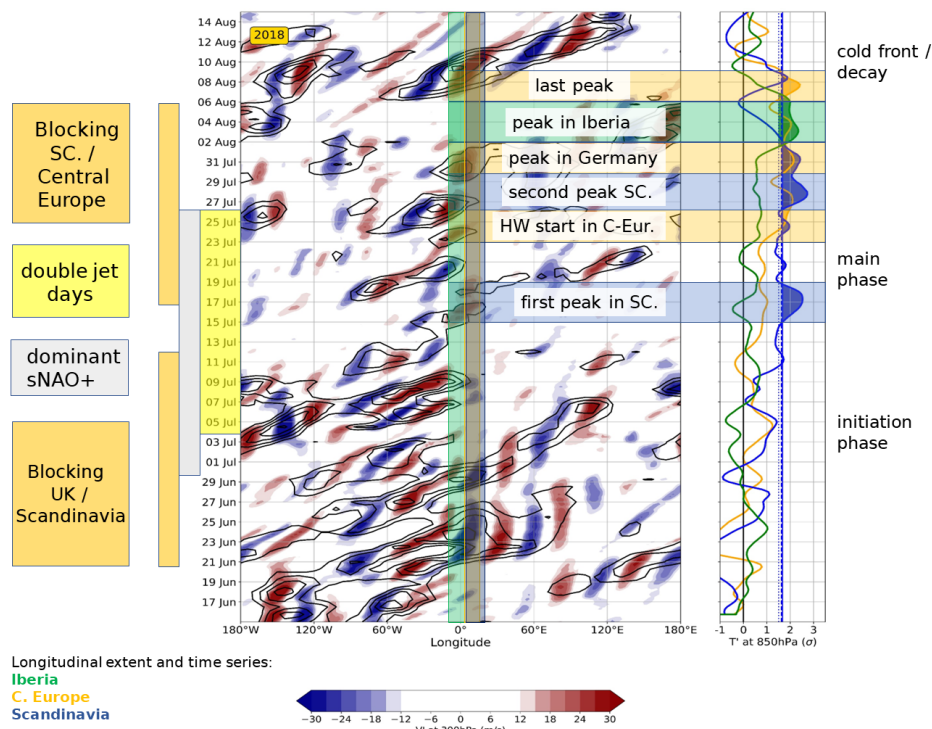
The analysis of Rossby wave activity permits the evaluation of the development of the blocking, NAO+ phase and the corresponding double jet structure for the summer 2018. Results show an eastward propagation of Rossby wave packets from the Pacific towards the Atlantic Ocean, the British Isles, and finally towards the European continent during the last 10 to 15 days of June and before the initiation of the heatwave over Scandinavia (Fig. 4). On the other hand, this was not the case for August, when the peak over Iberia occurred, which highlights the different mechanisms involved in this heatwave, rather than Rossby wave activity coming from the Pacific. Indeed, heatwaves and precipitation deficits in this location are primarily associated with amplified subtropical atmospheric ridges rather than midlatitude blocking situations (see Woollings et al., 2011; Sousa et al., 2017; 2018).

Further, a backward trajectory analysis was conducted to determine the origins of the air masses that were present during the different heatwave phases and their evolution. Three grid points were chosen to represent the three affected areas and time segments of the heatwave: one over Scandinavia (Utsjoki, Finland) initialized on 18 July 2018, one over central Europe (Bernburg, Germany) on 31 July, and one over Iberia (Alvega, Portugal) on 4 August 2018 (Fig. 5). The backward trajectories showed the remote origin of the mid-troposphere air masses, especially in the case of Utsjoki (Fig. 5a), where it primarily originated over the central North Atlantic. This is also true for the mid-troposphere air masses in the case of Bernburg (Fig. 5b). However, in the last 48 hours, descending air masses were





428 observed, pointing to an adiabatic warming by compression. Trajectories starting in the lowest 200 hPa  
429 at Bernburg, indicate that air masses stemmed from a region to the south and east close to the starting  
430 location, indicating relatively stagnant air masses as already discussed in Spensberger et al. (2020). In  
431 the case of Alvega (Fig. 5c), air masses starting between 700 and 1000 hPa experienced several rising  
432 and sinking motions on their way from the south and southeast (e.g. Algerian desert, Atlas Mountains,  
433 Mediterranean Sea), towards the Iberian plateau and coastal regions, thus documenting their local to  
434 regional origin and largely stagnant conditions (in line with Santos et al., 2015).  
435

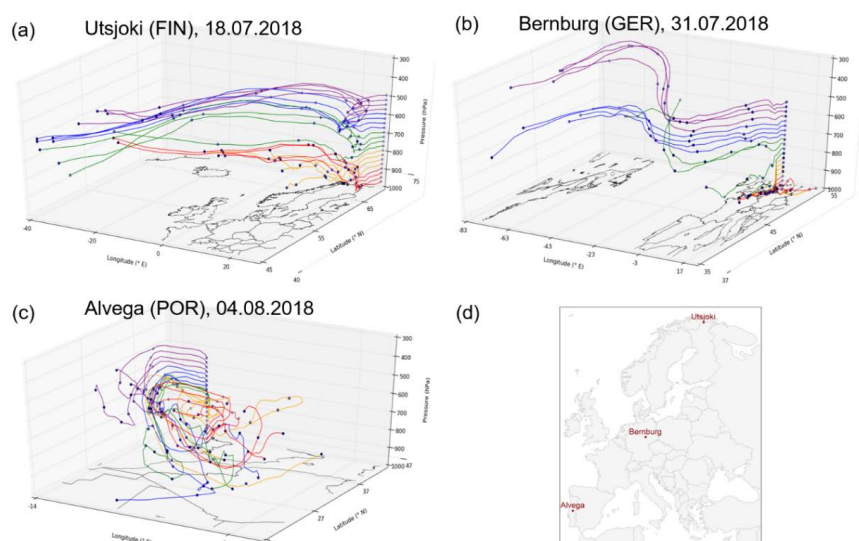


436  
437  
438 **Figure 4:** Hovmöller diagram for the period of 15.06.–15.08.2018. The longitudinal extent of three core  
439 heatwave regions (Iberia, Central Europe, Scandinavia), as well as their temperature time series at the  
440 850 hPa level as standardized anomalies ( $T'$ ) on the right, are marked in green, orange and blue,  
441 respectively. Periods when  $T'$  was above the respective 95th percentiles are shaded. Both temperature  
442 ( $T'$ ) and meridional wind at the 300 hPa level ( $v'$ ) are anomalies with respect to their smoothed annual  
443 cycles. Rossby wave packet amplitude ( $E$ ) is depicted in contours from 24 to 38 m/s in steps of 4 m/s,  
444  $v'$  as color shading from -30 to 30 m/s. Both fields are weighted by the cosine of latitude and  
445 meridionally averaged over above-median grid points within the 40-80° N latitude band (self-adjusting,  
446 depending on the location of the largest amplitudes). Days with a dominant positive phase of the





447 summer North Atlantic Oscillation (sNAO+) pattern, double jet days, and blocking days are marked on  
 448 the left.  
 449

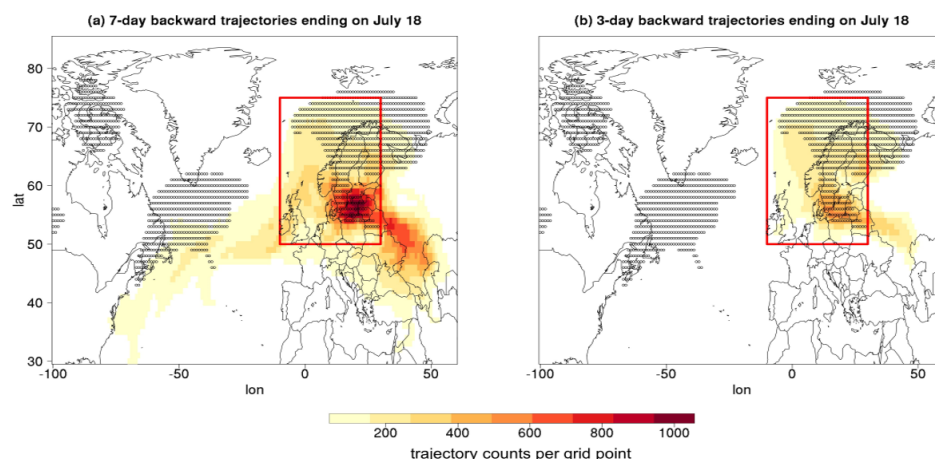


450  
 451 **Figure 5:** 10-day backward trajectories in 25 hPa steps between 1000 hPa and 500 hPa for the three  
 452 location coordinates. (a) Utsjoki, Finland, initialized 18.07.2018. (b) Bernburg, Germany, initialized  
 453 31.07.2018. (c) Alvega, Portugal, initialized 04.08.2018. For every 100 hPa, a different color is used for  
 454 the trajectories. Each black dot is representative of a 24-hour time step. (d) Geographical locations of  
 455 the three points.

456  
 457 In order to infer causal hypotheses for the existence of the Scandinavian block, the trajectory  
 458 approach was extended to obtain the origins of low potential vorticity (PV) air masses that formed the  
 459 upper-tropospheric part of the Scandinavian anticyclone (see Sect. 2.2.3). For the sake of brevity, only  
 460 maps of 7-day and 3-day trajectory density on 18 July 2018, around the maximum heatwave day in  
 461 Scandinavia, are shown in Figure 6, but other days corroborate the inferences below (not shown). Figure  
 462 6a shows the density of 7-day backward trajectories, indicating that air masses were steered from the  
 463 Western North Atlantic over the British Isles to Scandinavia. This is in line with the propagation of the  
 464 corresponding Rossby wave packet discussed above. Moreover, using the method described in  
 465 Zschenderlein et al. (2020, their Fig. 4), the role of a remote warm conveyor belt is suggested by  
 466 ascending, diabatically heated trajectories over the western Atlantic (not shown); PV is lowered in the  
 467 warm conveyor belt and then transported in the upper troposphere into the Scandinavian anticyclone  
 468 (termed “remote branch” by Zschenderlein et al. (2020). Interestingly, high trajectory densities over  
 469 central to eastern Europe, which also strongly ascended and were diabatically heated (not shown), point  
 470 towards an influence of moist convection observed under an upper-level trough in this area in feeding



low PV air towards the Scandinavian anticyclone. Such a “nearby branch” was also mentioned by Zschenderlein et al. (2020) to be important for anticyclone persistence over central Europe. However, in the 2018 case the nearby branch is located to the southeast, not to the southwest as for central Europe. Three days before the peak of the heatwave, trajectories almost exclusively stem from this nearby branch, now located more to the south of the Scandinavian anticyclone (Fig. 6b). Clearly, determining causal pathways from this analysis is not possible, yet modelling studies with explicit convection could shed more light on the role of the remote branch (warm conveyor belt over the western Atlantic) versus the nearby branch over southeastern Europe for the establishment and maintenance of the Scandinavian anticyclone.



480

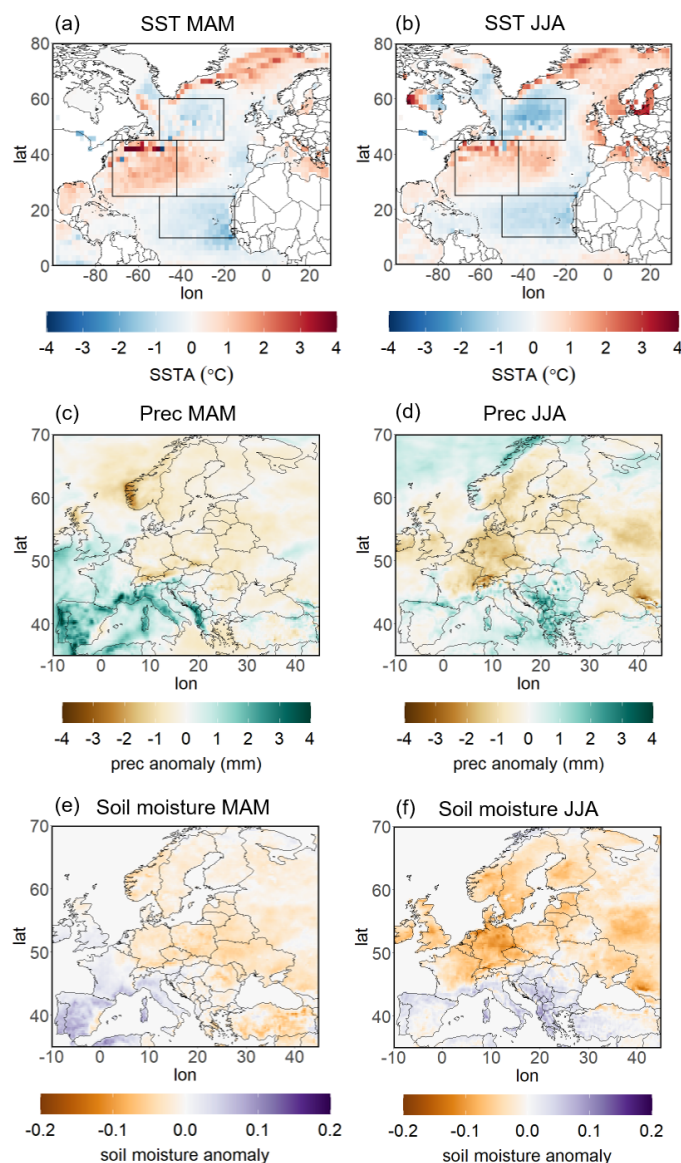
**Figure 6:** Backward trajectories for 7-days (a) and 3-days (b). Backward trajectory density maps ending on July 18, initiated in 50 hPa steps between 150 hPa and 500 hPa for grid points within the Scandinavian anticyclone (backward trajectories were initiated from the dotted points inside the red rectangle; the dotted points are those defined by vertically averaged PV anomaly based on monthly climatology  $< -0.7$  PVU and  $PV < 1$  PVU).

### 3.3 Low-frequency precursors

When addressing possible precursors for European heatwaves, SST anomalies over the North Atlantic (Ossó et al., 2020) and soil moisture anomalies over continental Europe (Quesada et al., 2012) are among the primary candidates, as outlined in the Introduction. A tripolar SST pattern with negative anomalies over the Subpolar Gyre (SPG) was evident in spring (MAM, northern box of Fig. 7a,b). At the same time, a pronounced precipitation deficit over Scandinavia in spring 2018 was present (Fig. 7c). The SST tripolar pattern persisted over time, with the cold SPG anomaly intensifying in summer (JJA, Fig. 7b), and the same is true for the precipitation deficit, which increased particularly in Germany and central Europe (Fig. 7d). The soil moisture anomaly for 2018 spring and summer (Fig. 7e,f) shows



495 a pattern consistent with the precipitation anomaly. LPJmL- simulated soil moisture anomalies for 2018  
 496 spring and summer (Fig. A5a,b) corroborate the spatial pattern seen in the ERA5 analysis.



497  
 498 **Figure 7:** Anomalies of sea surface temperature (SST; a,b), precipitation (c,d) and soil moisture (e, f)  
 499 in the ERA5 reanalysis (compared to the reference period 1981–2010) for spring (March to May; MAM;  
 500 a, c, e) and summer (June to August; JJA; b, d, f) months. Boxes in (a) and (b) indicate the regions for  
 501 the tripolar SST pattern.



502 Having established that the large-scale soil moisture anomaly is consistent with the SST and  
 503 precipitation anomalies, we investigated the temporal development of the soil moisture pattern over  
 504 Germany. Reduced soil moisture often facilitates the occurrence a summer drought and heatwaves, as  
 505 the soil moisture determinant for evapotranspiration (or lack thereof) directly links to the surface  
 506 temperature and relative humidity at the land surface. Thus, soil moisture and latent heat flux were used  
 507 to identify periods of moisture limitation (denoted by positive correlation coefficients between the two)  
 508 and wet conditions (negative correlation coefficients), under which the latent heat flux is primarily  
 509 controlled by the atmosphere. The derived (Fig. 8) and simulated (Fig. A5c,d) time series for the soil  
 510 moisture-latent heat flux correlations are based on daily data centered on 92-day running periods for  
 511 Germany. Additionally, centered 92-day running mean soil moisture is shown. The time series were  
 512 spatially averaged over all land points for northern (Fig. 8a,c; Fig. A5c,e) and southern Germany (Fig.  
 513 8b,d; Fig. A5d,f). Germany is usually not in the moisture-limited regime, but extraordinary hydrologic  
 514 conditions can lead to a shift from an energy-limited evaporative regime to moisture-limited conditions  
 515 (Lo et al., 2021), increasing the surface temperature and enhancing the sensible heat flux. The soil  
 516 moisture anomaly in March 2018 was low all over Germany (Fig. 8a,b; Fig. A5c,d; note that the LPJmL-  
 517 simulated soil moisture estimates are lower in absolute terms compared to ERA5, which is likely the  
 518 result of lower soil water holding capacity assumed in this model) and thus did not yet limit  
 519 evapotranspiration and latent heat flux. Warm conditions in spring caused a high latent heat flux all  
 520 over Germany, indicating a strong energy-limitation (Fig. 8c,d; Fig. A5e,f). High latent heat fluxes, in  
 521 turn, lead to a severe depletion of the soil moisture up to a depth of 1 m, starting at the end of March  
 522 and continuing until July in northern Germany and mid-August in southern Germany. The precipitation  
 523 deficit (Fig. 7c,d) further exacerbated the drying of the soils, and shifted the evaporative regime from  
 524 energy-limited to moisture-limited conditions. The latter prevailed between June and August 2018,  
 525 indicating that the anomalously dry soils during the 2018 summer further augmented the hot surface  
 526 temperatures (Dirmeyer et al., 2021; Orth, 2021).

527 In summary, the observed and modelled spring and early summer SST anomalies over the North  
 528 Atlantic and European soil moisture anomaly patterns for 2018 are in line with those identified for other  
 529 recent hot summers. Moreover, the dried-out soils and vegetation may have enhanced the maximum  
 530 temperatures by leading to anomalous latent heat fluxes.

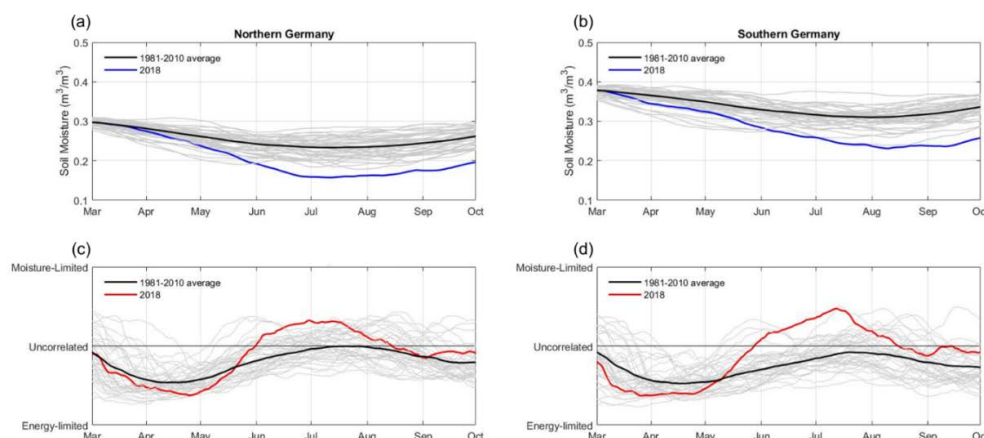


**Figure 8:** (a) Time series of centered 92-day running mean soil moisture averaged over all land points of northern Germany ( $51^{\circ}$  N –  $55^{\circ}$  N and  $4^{\circ}$  E –  $16^{\circ}$  E) for the period March-September of 1981-2020. The grey lines denote individual years, the black line the average of 1981-2010, and the blue line 2018. (b) As (a) but for southern Germany ( $48^{\circ}$  N- $51^{\circ}$  N and  $4^{\circ}$  E –  $16^{\circ}$  E). (c) Time series of soil moisture-latent heat flux coefficients based on 92-day running periods for the growing period covering March to September for the years 1981-2020 for northern Germany. The grey lines denote individual years, the black line the average of 1981-2010, and the red line 2018. Energy-limited is related to a correlation coefficient of -1, and moisture-limited to a correlation coefficient of 1. (d) As (c) but for southern Germany.

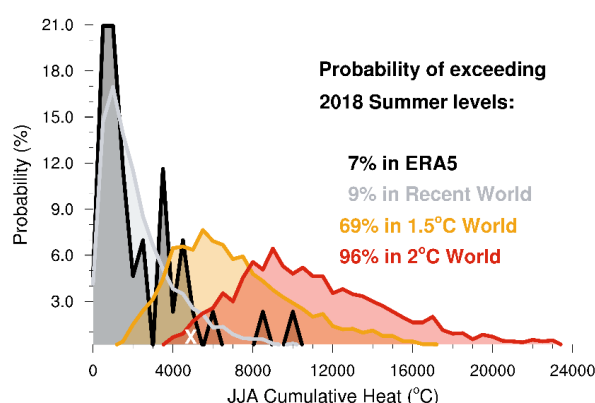
### 3.4 Attribution of the 2018 extreme heat

This section evaluates how anthropogenic climate change has affected the likelihood of similar heatwaves under present climate conditions and how it will affect their likelihood at global warming levels of  $+1.5^{\circ}$  C and  $+2^{\circ}$  C compared to pre-industrial times.

As defined by the cumulative heat metric, the 2018 summer was the 2nd warmest summer over Europe following 2010, surpassed again in 2019 and 2021 (not shown), ranking it 4<sup>th</sup> warmest by now, with 2022 being another candidate for warmest summer yet. In the period of 1950-2021, ERA5 data exhibits a 7 % likelihood of 2018 cumulative heat levels (black PDF in Fig. 9). MPI-GE, which is shown to adequately represent the variability and forced anthropogenic changes in observed temperatures (Suarez-Gutierrez et al., 2018; 2021), is also well able to capture cumulative heat (gray PDF in Fig. 9) as compared to ERA5. Under recent climate conditions, the 100 members of MPI-GE simulate a 9 % likelihood of exceeding 2018 levels, making this roughly a 1-in-10-years event. This is in line with an earlier attribution study by the World Weather Attribution (WWA) team who found return periods of about 1-in-10-years for Scandinavia and slightly less in the Netherlands (WWA, 2018). Under stronger global warming, this likelihood reaches 69 % in a  $+1.5^{\circ}$  C world, and 96 % in a  $+2^{\circ}$  C world (orange



556 and red PDFs in Fig. 9). Thus, conditions as extreme as the summer 2018 are projected to occur two  
 557 out of every three summers in a 1.5° C warmer world, while given 2° C of global warming they occur  
 558 virtually every single summer. The extreme summer 2018 represents a fairly average summer in a +1.5°  
 559 C world. In a 2° C warmer world, the cumulative heat during the average summer is twice as large as  
 560 the 2018 levels, while the most extreme 2° C world summers could exhibit more than four times more  
 561 excess heat compared to the recent climate conditions.



562  
 563 **Figure 9:** European ERA5 (1979-2021; black) cumulative heat versus MPI-GE under recent (1979-  
 564 2021; gray), future +1.5° C (2020-2049; orange), and +2° C (2050-2079; red) compared to pre-industrial  
 565 times warmer worlds. 2018 summer from ERA5 data is marked with white X. Daily maximum  
 566 temperatures (Tmax) for summer months (June to August; JJA) over land grid points only. Anomalies  
 567 with respect to 1981-2010. ERA5 data regridded to coarser resolution of MPI-GE. Probabilities are  
 568 normalized to percentages (divided by total number of years in period). Bin size is 500° C.

569  
 570 To estimate how much more likely the heat event of 2018 has become in Germany in recent decades  
 571 due to anthropogenic climate change, its probability ratio was calculated based on historical and his-  
 572 nat (pre-industrial-type) simulations from the CMIP6 archive. In a first step, we defined the extreme  
 573 event for which the tailored attribution analysis for Germany was conducted. We analyzed the  
 574 maximum daily temperature (Tmax) averaged for a box over Germany (47.5-55° N, 6-15° E) and to  
 575 account for the prolonged heat of 2018, we used the Tmax as a spatial average over seventeen days  
 576 (Tmax17). This length was defined based on the longest period of consecutive days with Tmax above  
 577 30 °C in German weather stations on record. Using this length, resulted in the longest return period.  
 578 Thus, annual block maxima of this variable (Tmax17) were constructed within the GEV fit and the  
 579 return periods were calculated. The return period of the 2018 summer Tmax17 (approximately 31° C  
 580 in E-OBS) was estimated as 108 years, making it a heatwave that is expected less than once in a lifetime  
 581 and can therefore have considerable impacts. It should be acknowledged that such a return period



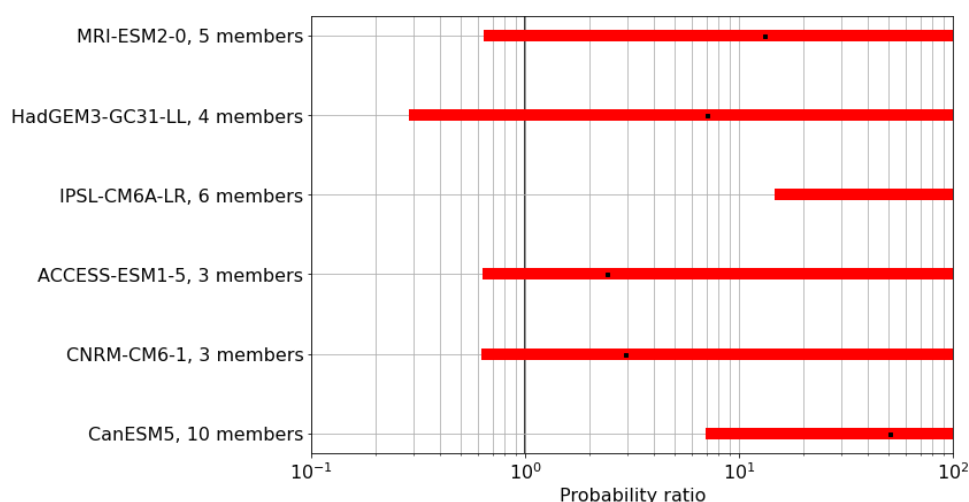


estimate contains uncertainties as the time series used to calculate it are shorter (about 70 years). Following the analysis of observation-based data, the following models were analyzed: CanESM5, CNRM-CM6-1, ACCESS-ESM1-5, IPSL-CM6A-LR, HadGEM3-GC31-LL, and MRI-ESM2-0 (see Table A1 for further details on the models used).

The probability ratio of the 2018 summer heatwave occurrence in Germany is shown for all analyzed models in Figure 10. For all models the probability ratio estimated on the original simulation data is larger than 1, meaning that the probability of such a heatwave has increased due to anthropogenic climate change. The red bars provide uncertainty ranges bases on the 1000 bootstraps. The best estimate in all analysed CMIP6 models (black squares) is  $> 2$ , again in line with the WWA findings despite a rather different event definition (WWA, 2018). For readability of the results, the x-axis in Figure 10 is only extended to a value of 100 with larger values omitted due to the large uncertainties. In fact, the upper range of probability ratios for some models is invalid as the event had a zero probability of occurrence in the hist-nat scenario, indicating that such an extended heatwave would have been very improbable under pre-industrial conditions.

In summary, the analysis of the impact of anthropogenic climate change on the heatwave in summer 2018 shows that such heat events have already become more frequent, i.e. their probability has increased compared to pre-industrial conditions. Furthermore, it is expected that such heat events will become even more likely in a warmer world.

600



601

**Figure 10:** Probability ratio (PR) of the 2018 summer heatwave occurrence in Germany in the analyzed CMIP6 models (see Table A1). The black squares show the PR estimated based on the original simulation time series and the red bars show the 5<sup>th</sup> to 95<sup>th</sup> PR percentiles calculated from a 1000-member bootstrap. The number of available DAMIP ensemble members is given together with the

605





606 model name and the originating institution on the y-axis. The vertical thick black line indicates a PR=1,  
 607 above which the likelihood of such an event has increased compared to pre-industrial times.

608  
 609 Drought attribution is notoriously difficult due to the fact that global models only crudely reproduce  
 610 convective precipitation, which is the main mode of rainfall in summer. While evapotranspiration is  
 611 increasing with warming, the question whether or not this can be compensated by stronger downpours  
 612 to avoid hydrological (or agricultural) drought cannot be answered with any degree of certainty at the  
 613 moment. Drought episodes are expected to increase (Masson-Delmotte et al. IPCC, 2021) across the  
 614 world, but the frequency of occurrence and the actual change in risk cannot be quantified yet.  
 615 Nevertheless, it is likely that the prolonged 2018 drought, followed by two more below-average rainfall  
 616 years in 2019 and 2020 in Germany, is partially attributable to human-induced climate change. Given  
 617 that attributable global warming is approximately 1.1° C (2011-2020), corresponding to 100% of the  
 618 observed warming and warming over land is much more rapid, Europe has already warmed by ~2°C,  
 619 with summer warming being particularly amplified due to soil moisture feedbacks with increased  
 620 sensible heat flux. Together with the potential dynamic feedback discussed above, the average summer  
 621 Tmax in Europe may well exceed 3° C above pre-industrial conditions already. This is corroborated by  
 622 a recent WWA study which analyzed the recent UK heat record and found that climate change added  
 623 4° C to the observed record Tmax. What used to be a 36°C day is now a 40°C day (World Weather  
 624 Attribution (WWA), 2022).

#### 625 **4 Discussion and conclusions**

626 The extreme heat and drought of the summer 2018 has been studied from a multi-faceted weather  
 627 and climate perspective. We looked at hot and dry summers over Europe using different analysis  
 628 approaches to study the extremeness and attribution to anthropogenic climate change (climate  
 629 perspective), as well as synoptic dynamics in concert with slowly varying boundary conditions at the  
 630 ocean and continental surfaces (seasonal and weather perspective). The 2018 summer is found to be a  
 631 unique historical example of persistent heatwave and drought conditions in large parts of Europe. This  
 632 is particularly true for northern and central Europe, regions which - unlike the seasonal drought in the  
 633 Mediterranean- are historically not so accustomed to this kind of concurrent hot and dry summer  
 634 extremes. The 2018 summer is one more case in a cluster of intense heatwaves facing Europe over the  
 635 last decades (Russo et al., 2015; Becker et al., 2022). The 2018 drought was an intense, large-scale  
 636 event, promoting strong land-atmosphere coupling that exacerbated the heatwave (Dirmeyer et al.,  
 637 2021).

638 Regarding the large-scale atmospheric conditions conducive of the summer 2018 extremes, we  
 639 provided detailed evidence on the blocking anticyclones, persistent double jet stream configurations,  
 640 sNAO+ phase, Rossby wave activity, and different air mass origins. For example, the persistent double



641 jet stream event, combined with record high positive sNAO (Drouard et al., 2019), seems to have played  
 642 a role in the long duration of the 2018 heatwave. Additionally, according to Li et al. (2020), the  
 643 collaborative (not mutually exclusive) roles of sNAO+ and European blocking could favor the  
 644 frequency, persistence, and magnitude of heatwaves over Europe, as the sNAO+ related blocking events  
 645 are quasi-stationary and more persistent compared to the non-NAO+ related ones. Evidence is provided  
 646 regarding the origin of the low PV air masses in the upper-tropospheric blocking anticyclone over  
 647 Scandinavia; while in its initiation phase, backward trajectory analyses point to a role of a western North  
 648 Atlantic warm conveyor belt, we provide hints that its maintenance could be supported by low PV air  
 649 stemming from moist convection in the trough flanking the block to its southeast, i.e. over Eastern  
 650 Europe. However, further analysis is needed to address the direction of causality behind this link. On  
 651 the other hand, our analysis suggests that the later heatwave phase over Iberia has different drivers, as  
 652 the air masses originated locally or were advected from nearby areas (e.g. North Africa) and are not  
 653 necessarily directly associated with the propagation and breaking of large-scale Rossby waves as over  
 654 Scandinavia (Santos et al., 2015; Sousa et al., 2019).

655 The dominant oceanic and large-scale conditions of the North Atlantic might have supported the  
 656 development of the 2018 heatwave. The physical reasoning on the relationship between the North  
 657 Atlantic SST tripole and exceptionally cold North Atlantic ocean, the jet stream set up and the  
 658 occurrence of the heat wave was proposed by Duchez et al. (2016) based on the summer 2015 event.  
 659 Here, we documented that similar anomalies were also observed during the spring of 2018. While the  
 660 atmospheric forcing is associated with the anomalous jet stream positions and blocking, they in turn  
 661 influence the precipitation patterns over Europe, leading to changes in the soil moisture content.  
 662 Although such a process enhances the potential for a heat extreme, the meteorological factors are the  
 663 ones that determine the timing and duration of the heatwave. Dedicated modeling experiments and  
 664 causal inference algorithms will be key to test the hypothesis of a causal link between spring North  
 665 Atlantic SSTs and subsequent summer extremes in Europe. Moreover, the patterns of North Atlantic  
 666 SSTs are acting on top of the warming background climate, which may further modify the type or the  
 667 magnitude of those relationships (McCarthy et al., 2019).

668 The severe soil moisture depletion in Germany between April and July of 2018 reflected the  
 669 persistently warm and dry conditions and led to anomalously dry soils in summer. The drought  
 670 conditions in the soil pushed its state into the transition zone conditions, in which soil wetness plays a  
 671 direct role in influencing the climate by reducing the evaporative cooling effect at the land surface and  
 672 thus enhancing hot and dry conditions. The moisture-limited conditions that prevailed between June  
 673 and August 2018 indicated that the hot surface temperatures are directly linked to anomalously dry soils  
 674 during the 2018 summer period (Dirmeyer et al., 2021; Orth, 2021).

675 We also showed that summer 2018 was extreme in the observational record for Europe and that  
 676 heat anomalies of this magnitude are expected to occur much more often in a warmer world, being  
 677 reached up to almost every year with global warming of +2° C. Wehrli et al. (2020) provided evidence



that the anthropogenic background warming was a strong contributor to the 2018 summer heatwave in the Northern Hemisphere, highlighting that future extremes under similar atmospheric circulation conditions at higher levels of global warming would reach dangerous levels. Our tailored attribution study, which analyzed how the maximum temperature, averaged over 17 days over Germany, has been impacted by anthropogenic climate change, showed that the probability of such a prolonged heat event has increased in all CMIP6 models analyzed here. Attribution studies that analyzed the summer 2018 heatwave in other areas of Europe also found an increase in its likelihood under anthropogenic climate change (McCarthy et al., 2019; Vogel et al., 2019; Leach et al., 2020).

We have presented a comprehensive study of the extreme hot and dry 2018 summer in Europe, investigating its emergence and evolution with a combination of conventional and more sophisticated metrics and methods, with an emphasis on their synoptic-scale atmospheric drivers and a reference to their potential precursors in spring. Moreover, by assessing the event from a climate perspective, we provided evidence that anomalous summers of such extremity have already, and will further, become much more frequent in a warming world. Overall, this study highlights the added value of multi-faceted approaches for the analysis of such extreme events, and that collaboration among different fields is crucial both for the process understanding and the subsequent quantification of impacts. At the time of writing in 2022, yet another, potentially more extreme hot and dry summer is affecting Europe corroborating the approach of this study, but also emphasizing the need to carry out multi-disciplinary impact studies.

## Appendix

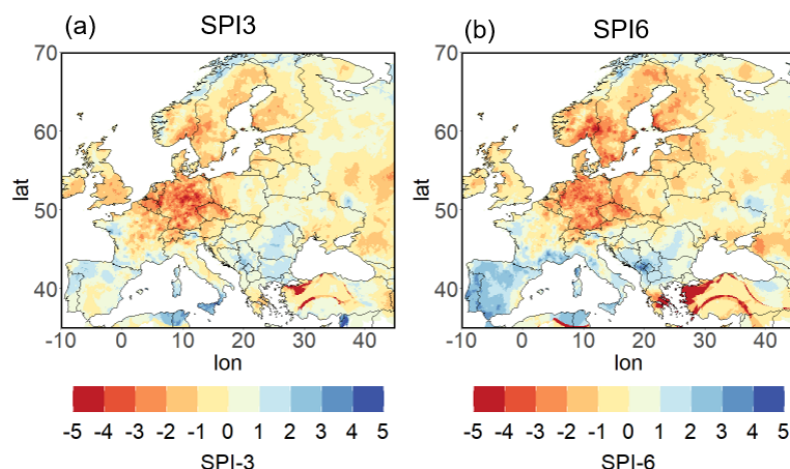
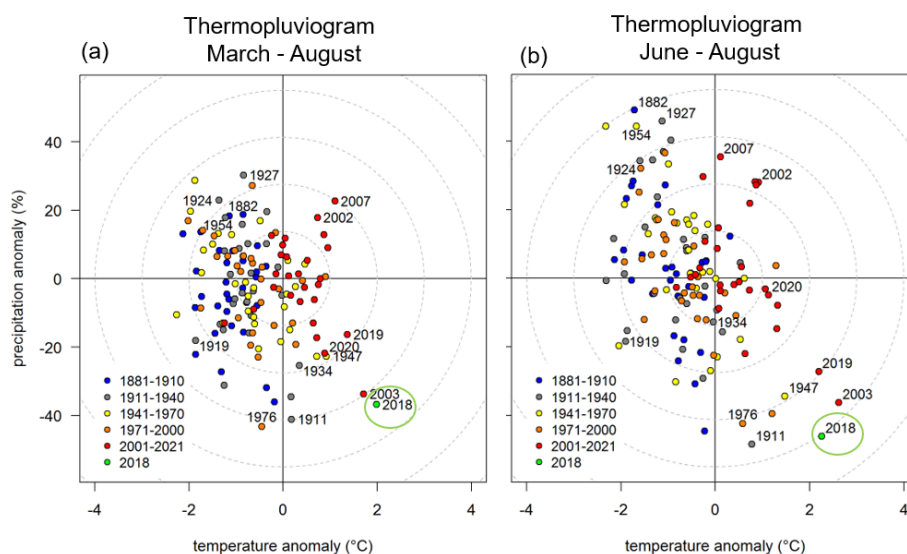
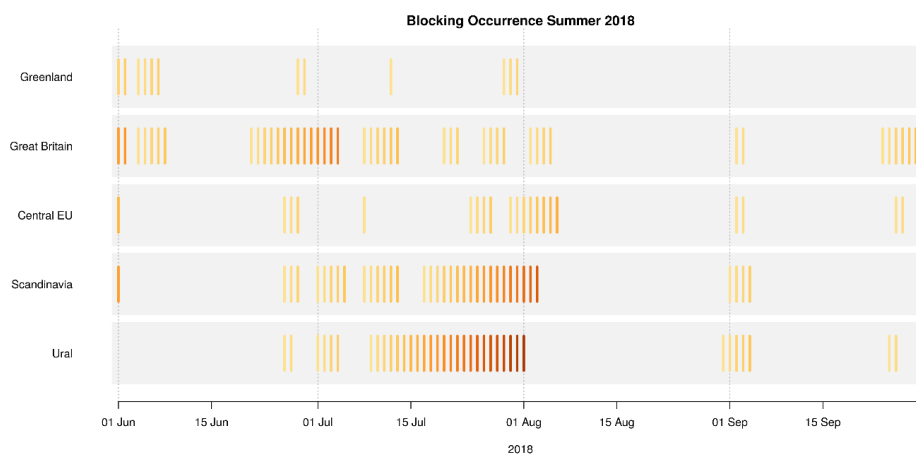


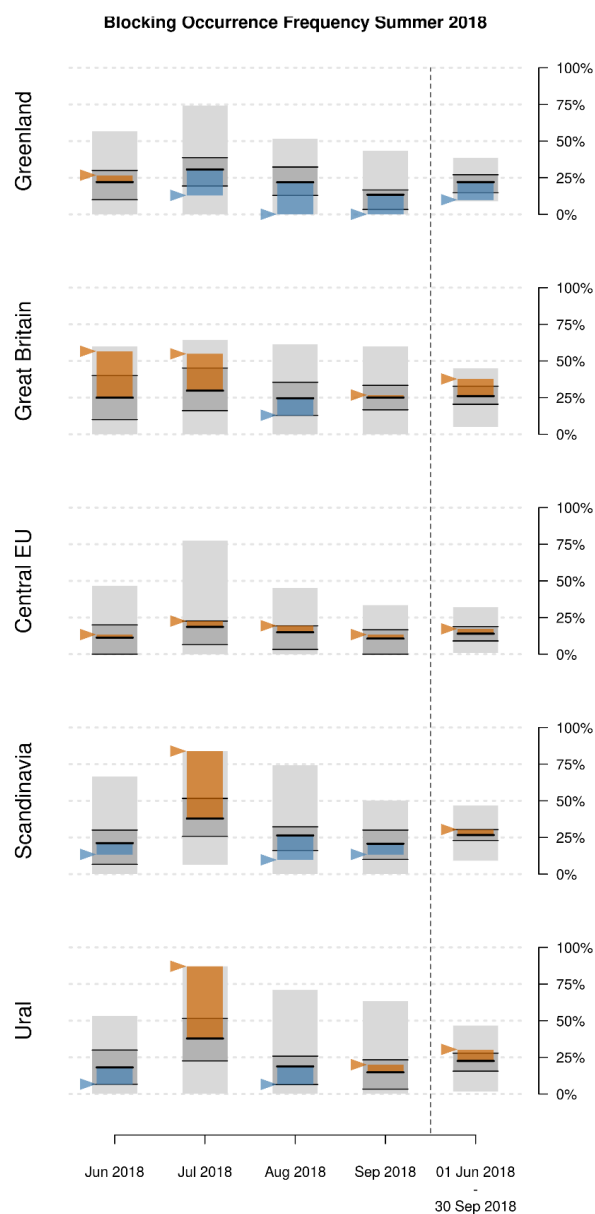
**Figure A1:** SPI3 and SPI6 August 2018 (E-OBS data, reference period 1981-2010).



700  
 701 **Figure A2:** Thermopluviogram for Germany for the March – August (a) and for June-August  
 702 (c). Values of temperature and precipitation anomalies from the climatological mean shown  
 703 for 30-year periods of 1881-2021 (reference period 1981-2010). 2018 is highlighted with light  
 704 green color.



705  
 706 **Figure A3:** Daily atmospheric blocking occurrence and duration of consecutive blocked days  
 707 (colored bars; increasing from orange to red) in different European regions from June to  
 708 September 2018 in ERA5 reanalysis data. A day is defined as blocked if an area of at least 1  
 709 million km<sup>2</sup> of the specific region is blocked based on the 2-dimensional blocking index  
 710 described in 2.2.3.



711  
 712 **Figure A4:** Monthly regional blocking frequency (fraction of blocked days) from June to  
 713 September 2018 (colored bars and arrows) compared to climatological blocking frequencies  
 714 from 1950 to 2020 in ERA5 reanalysis data. Black horizontal lines indicate the mean, light  
 715 (dark) gray bars the minimum and maximum (25% and 75% quantiles) of historical blocking  
 716 frequencies. Derived blocking frequencies are based on the definition of blocked days given in  
 717 Figure A3.

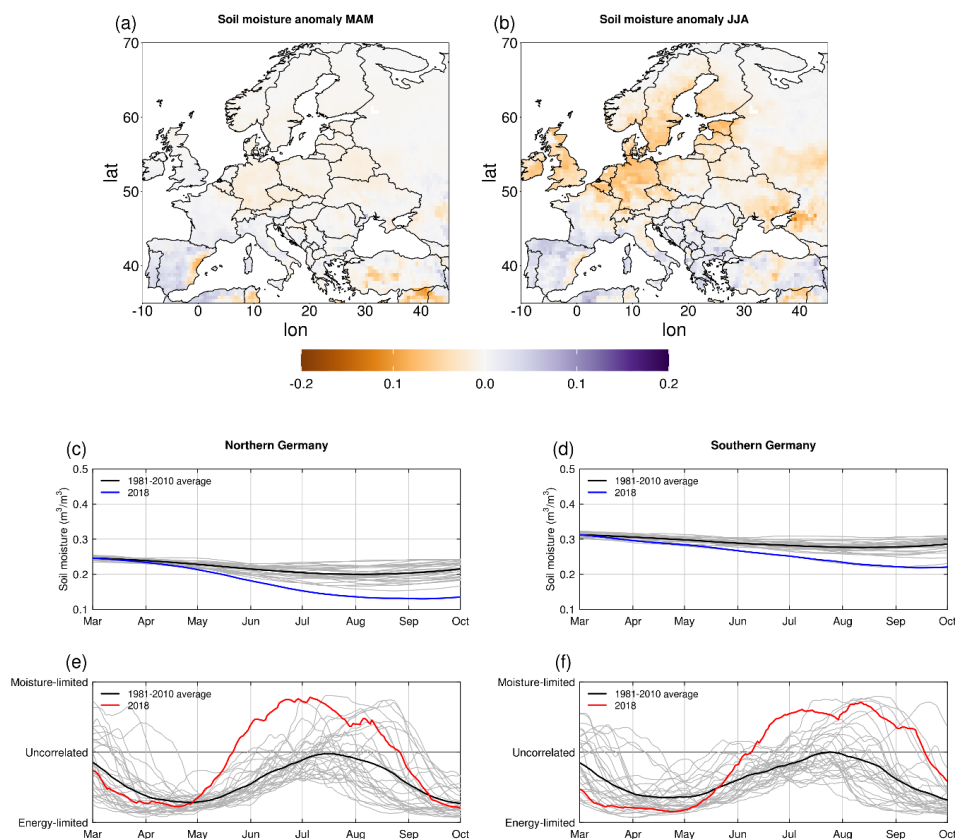


**Figure A5:** Soil moisture as simulated by LPJmL with bias-adjusted ERA5 climate forcing. Anomalies of soil moisture for (a) March to May (MAM) and (b) June to August (JJA) as compared to the reference period of 1981–2010. Time series of centered 92-day running mean soil moisture averaged over all land points of (c) northern Germany (51 °N – 55 °N and 4 °E – 16 °E) and (d) southern Germany (48 °N–51 °N and 4 °E – 16 °E) for the growing period March–September of 1981–2020. The grey lines denote individual years, the black line the average of 1981–2010, and the blue line 2018. Time series of soil moisture-latent heat flux coefficients based on 92-day running periods for the growing period covering March to September for the years 1981–2020 for (e) northern Germany and (f) southern Germany; the grey lines denote individual years, the black line the average of 1981–2010, and the red line 2018. Energy-limited is related to a correlation coefficient of -1, and moisture-limited to a correlation coefficient of 1.

**Table A1:** CMIP6 models used for the heatwave attribution over Germany. CMIP source\_id, institution\_id, data versions for the historical and hist-nat simulations, and data citation for the CMIP6/DAMIP simulations used in the attribution study. Where initializations of the same model were



735 using more than one model identifying version, all of them are given and the one that was used for most  
 736 initializations is marked in bold, where possible.

source_id	institution_id	Versions historical / version hist- nat	Versions hist-nat	Data citation historical	Data citation hist-nat
MRI-ESM2-0	MRI	<b>v20190603</b> v20200327, v20201029	<b>v20190603</b> v20200415	Yukimoto et al., 2019	Yukimoto et al., 2019b
HadGEM3- GC31-LL	MOHC NERC 2016	<b>v20190624</b> v20190626	v20190726, v20190729, v20190730, v20190805	Ridley et al., 2019	Jones, 2019
IPSL-CM6A-LR	IPSL	<b>v20190614</b> v20190802	v20190614	Boucher et al., 2018	Boucher et al., 2018b
ACCESS- ESM1-5	CSIRO	v20191115, v20191128, v20191203, v20200529, v20200601, v20200605, <b>v20200803</b>	v20200615	Ziehn et al., 2019	Ziehn et al., 2020
CNRM-CM6-1	CNRM- CERFACS	v20180917, v20181126, v20190125, <b>v20191004</b> , v20200529	v20190308	Voldoire, 2018	Voldoire, 2019
CanESM5	CCCma	v20190429 / v20190429	v20190429	Swart et al., 2019	Swart et al., 2019b

#### 737 **Code availability**

738 Code is available from the authors upon request.

#### 739 **Data availability**

740 The source of all datasets is listed in text and references. Further information can be made available  
 741 upon request to the corresponding authors.

#### 742 **Competing interests**

743 The authors declare no competing interests.

#### 744 **Author Contribution**

745 ER and AF coordinated the inter-disciplinary task force on heat and drought within ClimXtreme and  
 746 this collaborative paper; ER did the jet stream analysis, prepared Figures 1, 3c, 5d, 7, A1 and curated





747 most of the final figures with contributions from different co-authors (see below), and wrote the first  
 748 draft of the paper with contributions from different co-authors; FB calculated UTCI, did the Rossby  
 749 wave packet and the trajectories analysis and prepared Figures 4, 5, 6; GBA calculated the cumulate  
 750 heat metric in ERA5 and the SST anomalies; DP calculated SPEI and SPI; MB did the regional climate  
 751 network analysis and prepared Figure 2a; DN and SS prepared Figure 2b and A2; AR did the blocking  
 752 analysis and prepared Figures 3a,b, A3, and A4; JR did the weather regime analysis; LJ calculated  
 753 precipitation and soil moisture anomalies in ERA5 and prepared Figure 8; LSA and JH modeled soil  
 754 moisture with LPJmL and prepared Figure A5; LSG did the MPI-GE attribution study and prepared  
 755 Figure 9; JT did the CMIP6 attribution study and prepared Figure 10 and Table A1; GC contributed to  
 756 the CMIP6 attribution study. All authors followed the analysis from the beginning, contributed text and  
 757 edited/commented the final version of the manuscript.

## 758 Acknowledgements

759 This paper is a collaborative effort within the BMBF ClimXtreme project, for which the authors  
 760 acknowledge funding (grant numbers 01LP1901A, 01LP1901C, 01LP191D, 01LP1901E, 01LP1902F,  
 761 01LP1903J, 01LP1902D, 01LP1902N, 01LP1903C, 01LP1902B, 01LP1904A). AD is supported by A4  
 762 (Aigéin, Aeráid, agus athrú Atlantaigh), funded by the Marine Institute (grant PBA/CC/18/01). EX  
 763 acknowledges support by the H2020 Project CLINT, the Academy of Athens and the Greek “National  
 764 Research Network on Climate Change and its Impact” (200/937). GF acknowledges the support of the  
 765 German Research Foundation (DFG; project no. 445572993). JGP thanks the AXA research fund for  
 766 support. We acknowledge the World Climate Research Programme, which, through its Working Group  
 767 on Coupled Modelling, coordinated and promoted CMIP6. We thank the climate modeling groups for  
 768 producing and making available their model output, the Earth System Grid Federation (ESGF) for  
 769 archiving the data and providing access, and the multiple funding agencies who support CMIP6 and  
 770 ESGF. We acknowledge the E-OBS dataset from the EU-FP6 project UERRA (<http://www.uerra.eu>)  
 771 and the Copernicus Climate Change Service, and the data providers in the ECA&D project  
 772 (<https://www.ecad.eu>).

## 773 References

- 774 Allen, R. G., Pruitt, W. O., Wright, J. L., Howell, T. A., Ventura, F., Snyder, R., Itenfisu, D., Steduto,  
 775 P., Berengena, J., Yrisarry, J. B., Smith, M., Pereira, L. S., Raes, D., Perrier, A., Alves, I., Walter, I.  
 776 and Elliott, R.: A recommendation on standardized surface resistance for hourly calculation of  
 777 reference ETo by the FAO56 Penman-Monteith method, *Agric. Water Manag.*, 81(1–2), 1–22,  
 778 doi:10.1016/J.AGWAT.2005.03.007, 2006.
- 779 Bakke, S. J., Ionita, M. and Tallaksen, L. M.: The 2018 northern European hydrological drought and  
 780 its drivers in a historical perspective, *Hydrol. Earth Syst. Sci.*, 24(11), 5621–5653, doi:10.5194/hess-  
 781 24-5621-2020, 2020.
- 782 Barriopedro, D., Fischer, E. M., Luterbacher, J., Trigo, R. M. and García-Herrera, R.: The hot summer



- 783 of 2010: Redrawing the temperature record map of Europe, *Science* (80-. ), 332(6026), 220–224,  
 784 doi:10.1126/SCIENCE.1201224/SUPPL\_FILE/PAP.PDF, 2011.
- 785 Barriopedro, D., Sousa, P. M., Trigo, R. M., García-Herrera, R. and Ramos, A. M.: The exceptional  
 786 Iberian heatwave of summer 2018, *Bull. Am. Meteorol. Soc.*, 101(1), S29–S34, doi:10.1175/BAMS-  
 787 D-19-0159.1, 2020.
- 788 Bastos, A., Ciais, P., Friedlingstein, P., Sitch, S., Pongratz, J., Fan, L., Wigneron, J. P., Weber, U.,  
 789 Reichstein, M., Fu, Z., Anthoni, P., Arneeth, A., Haverd, V., Jain, A. K., Joetzjer, E., Knauer, J.,  
 790 Lienert, S., Loughran, T., McGuire, P. C., Tian, H., Viovy, N. and Zaehle, S.: Direct and seasonal  
 791 legacy effects of the 2018 heat wave and drought on European ecosystem productivity, *Sci. Adv.*,  
 792 6(24), doi:10.1126/sciadv.aba2724, 2020.
- 793 Bastos, A., Orth, R., Reichstein, M., Ciais, P., Viovy, N., Zaehle, S., Anthoni, P., Arneeth, A., Gentile,  
 794 P., Joetzjer, E., Lienert, S., Loughran, T., McGuire, P., O, S., Pongratz, J. and Sitch, S.: Increased  
 795 vulnerability of European ecosystems to two compound dry and hot summers in 2018 and 2019, *Earth*  
 796 *Syst. Dyn. Discuss.*, 1–32, doi:10.5194/esd-2021-19, 2021.
- 797 Becker, F. N., Fink, A. H., Bissolli, P. and Pinto, J. G.: Towards a more comprehensive assessment of  
 798 the intensity of historical European heat waves (1979–2019), *Atmos. Sci. Lett.*, e1120,  
 799 doi:10.1002/ASL.1120, 2022.
- 800 Beguería, S. and Vicente-Serrano, S. M.: SPEI: Calculation of Standardized Precipitation-  
 801 Evapotranspiration Index, R package version 1.6, [online] Available from:  
 802 <https://www.rdocumentation.org/packages/SPEI/versions/1.6/topics/SPEI-package>, 2013.
- 803 Beilouin, D., Schauburger, B., Bastos, A., Ciais, P. and Makowski, D.: Impact of extreme weather  
 804 conditions on European crop production in 2018, *Philos. Trans. R. Soc. B*, 375(1810),  
 805 doi:10.1098/RSTB.2019.0510, 2020.
- 806 Błazejczyk, K., Jendritzky, G., Bröde, P., Fiala, D., Havenith, G., Epstein, Y., Psikuta, A. and  
 807 Kampmann, B.: An introduction to the Universal thermal climate index (UTCI), *Geogr. Pol.*, 86(1),  
 808 5–10, doi:10.7163/GPol.2013.1, 2013.
- 809 Von Bloh, W., Schaphoff, S., Müller, C., Rolinski, S., Waha, K. and Zaehle, S.: Implementing the  
 810 nitrogen cycle into the dynamic global vegetation, hydrology, and crop growth model LPJmL (version  
 811 5.0), *Geosci. Model Dev.*, 11(7), 2789–2812, doi:10.5194/GMD-11-2789-2018, 2018.
- 812 Boucher, O., Denvil, S., Levvasseur, G., Cozic, A., Caubel, A., Foujols, M.-A., Meurdesoif, Y.,  
 813 Cadule, P., Devilliers, M., Ghattas, J., Lebas, N., Lurton, T., Mellul, L., Musat, I., Mignot, J. and  
 814 Cheruy, F.: IPSL IPSL-CM6A-LR model output prepared for CMIP6 CMIP historical, ,  
 815 doi:10.22033/ESGF/CMIP6.5195, 2018a.
- 816 Boucher, O., Denvil, S., Levvasseur, G., Cozic, A., Caubel, A., Foujols, M.-A., Meurdesoif, Y. and  
 817 Gastineau, G.: IPSL IPSL-CM6A-LR model output prepared for CMIP6 DAMIP hist-nat, ,  
 818 doi:10.22033/ESGF/CMIP6.13831, 2018b.
- 819 Di Capua, G., Sparrow, S., Kornhuber, K., Rousi, E., Osprey, S., Wallom, D., van den Hurk, B. and  
 820 Coumou, D.: Drivers behind the summer 2010 wave train leading to Russian heatwave and Pakistan  
 821 flooding, *npj Clim. Atmos. Sci.*, 4(1), 55, doi:10.1038/s41612-021-00211-9, 2021.
- 822 Chen, S., Wu, R. and Liu, Y.: Dominant Modes of Interannual Variability in Eurasian Surface Air  
 823 Temperature during Boreal Spring, *J. Clim.*, 29(3), 1109–1125, doi:10.1175/JCLI-D-15-0524.1, 2016.
- 824 Climate Change Service: Dry and warm spring and summer, [online] Available from:  
 825 <https://climate.copernicus.eu/dry-and-warm-spring-and-summer>, 2018.
- 826 Climate Change Service: Warmest summer for Europe by small margin; August globally joint third  
 827 warmest on record, [online] Available from: [https://climate.copernicus.eu/copernicus-warmest-](https://climate.copernicus.eu/copernicus-warmest-small-margin-europe-small-margin-august-globally-joint-third-warmest-record)  
 828 [small-margin-europe-small-margin-august-globally-joint-third-warmest-record](https://climate.copernicus.eu/copernicus-warmest-small-margin-europe-small-margin-august-globally-joint-third-warmest-record), 2021.
- 829 Cornes, R. C., van der Schrier, G., van den Besselaar, E. J. M. and Jones, P. D.: An Ensemble Version  
 830 of the E-OBS Temperature and Precipitation Data Sets, *J. Geophys. Res. Atmos.*, 123(17), 9391–  
 831 9409, doi:10.1029/2017JD028200, 2018.
- 832 Crasemann, B., Handorf, D., Jaiser, R., Dethloff, K., Nakamura, T., Ukita, J. and Yamazaki, K.: Can  
 833 preferred atmospheric circulation patterns over the North-Atlantic-Eurasian region be associated with  
 834 arctic sea ice loss?, *Polar Sci.*, 14, 9–20, doi:10.1016/J.POLAR.2017.09.002, 2017.
- 835 Dirmeyer, P. A., Balsamo, G., Blyth, E. M., Morrison, R. and Cooper, H. M.: Land-Atmosphere  
 836 Interactions Exacerbated the Drought and Heatwave Over Northern Europe During Summer 2018,  
 837 *AGU Adv.*, 2(2), e2020AV000283, doi:10.1029/2020AV000283, 2021.



- 838 Donges, J. F., Zou, Y., Marwan, N. and Kurths, J.: Complex networks in climate dynamics, *Eur. Phys.*
- 839 *J. Spec. Top.* 2009 1741, 174(1), 157–179, doi:10.1140/EPJST/E2009-01098-2, 2009.
- 840 Droogers, P. and Allen, R. G.: Estimating Reference Evapotranspiration Under Inaccurate Data
- 841 Conditions, *Irrig. Drain. Syst.* 2002 161, 16(1), 33–45, doi:10.1023/A:1015508322413, 2002.
- 842 Drouard, M., Kornhuber, K. and Woollings, T.: Disentangling Dynamic Contributions to Summer
- 843 2018 Anomalous Weather Over Europe, *Geophys. Res. Lett.*, 46(21), 12537–12546,
- 844 doi:10.1029/2019GL084601, 2019.
- 845 Duan, S. Q., Findell, K. L. and Wright, J. S.: Three Regimes of Temperature Distribution Change
- 846 Over Dry Land, Moist Land, and Oceanic Surfaces, *Geophys. Res. Lett.*, 47(24), e2020GL090997,
- 847 doi:10.1029/2020GL090997, 2020.
- 848 Duchez, A., Frajka-Williams, E., Josey, S. A., Evans, D. G., Grist, J. P., Marsh, R., McCarthy, G. D.,
- 849 Sinha, B., Berry, D. I. and Hirschi, J. J. M.: Drivers of exceptionally cold North Atlantic Ocean
- 850 temperatures and their link to the 2015 European heat wave, *Environ. Res. Lett.*, 11(7), 1–9,
- 851 doi:10.1088/1748-9326/11/7/074004, 2016.
- 852 Eyring, V., Bony, S., Meehl, G. A., Senior, C. A., Stevens, B., Stouffer, R. J. and Taylor, K. E.:
- 853 Overview of the Coupled Model Intercomparison Project Phase 6 (CMIP6) experimental design and
- 854 organization, *Geosci. Model Dev.*, 9(5), 1937–1958, doi:10.5194/GMD-9-1937-2016, 2016.
- 855 Fink, A. H., Brücher, T., Krüger, A., Leckebusch, G. C., Pinto, J. G. and Ulbrich, U.: The 2003
- 856 European summer heatwaves and drought –synoptic diagnosis and impacts, *Weather*, 59(8), 209–216,
- 857 doi:10.1256/wea.73.04, 2004.
- 858 Fischer, E. M. and Schär, C.: Consistent geographical patterns of changes in high-impact European
- 859 heatwaves, *Nat. Geosci.*, 3(6), 398–403, doi:10.1038/ngeo866, 2010.
- 860 Folland, C. K., Knight, J., Linderholm, H. W., Fereday, D., Ineson, S. and Hurrell, J. W.: The summer
- 861 North Atlantic oscillation: Past, present, and future, *J. Clim.*, 22(5), 1082–1103,
- 862 doi:10.1175/2008JCLI2459.1, 2009.
- 863 Fragkoulidis, G. and Wirth, V.: Local rossby wave packet amplitude, phase speed, and group velocity:
- 864 Seasonal variability and their role in temperature extremes, *J. Clim.*, 33(20), 8767–8787,
- 865 doi:10.1175/JCLI-D-19-0377.1, 2020.
- 866 Friedrich, K. and Kaspar, F.: Rückblick auf das Jahr 2018 – das bisher wärmste Jahr in Deutschland,
- 867 [online] Available from:
- 868 [https://www.dwd.de/DE/leistungen/besondereereignisse/temperatur/20190102\\_waermstes\\_jahr\\_in\\_de](https://www.dwd.de/DE/leistungen/besondereereignisse/temperatur/20190102_waermstes_jahr_in_deutschland_2018.pdf?__blob=publicationFile&v=2)
- 869 [utschland\\_2018.pdf?\\_\\_blob=publicationFile&v=2](https://www.dwd.de/DE/leistungen/besondereereignisse/temperatur/20190102_waermstes_jahr_in_deutschland_2018.pdf?__blob=publicationFile&v=2) am: 10.12.2021 (Accessed 4 April 2022), 2019.
- 870 Gastineau, G. and Frankignoul, C.: Influence of the North Atlantic SST variability on the atmospheric
- 871 circulation during the twentieth century, *J. Clim.*, 28(4), 1396–1416, doi:10.1175/JCLI-D-14-00424.1,
- 872 2015.
- 873 Gillett, N. P., Shiogama, H., Funke, B., Hegerl, G., Knutti, R., Matthes, K., Santer, B. D., Stone, D.
- 874 and Tebaldi, C.: The Detection and Attribution Model Intercomparison Project (DAMIP v1.0)
- 875 contribution to CMIP6, *Geosci. Model Dev.*, 9(10), 3685–3697, doi:10.5194/GMD-9-3685-2016,
- 876 2016.
- 877 Haylock, M. R., Hofstra, N., Klein Tank, A. M. G., Klok, E. J., Jones, P. D. and New, M.: A
- 878 European daily high-resolution gridded data set of surface temperature and precipitation for 1950–
- 879 2006, *J. Geophys. Res. Atmos.*, 113(D20), 20119, doi:10.1029/2008JD010201, 2008.
- 880 Heim, R. R.: A Review of Twentieth-Century Drought Indices Used in the United States, *Bull. Am.*
- 881 *Meteorol. Soc.*, 83(8), 1149–1166, doi:10.1175/1520-0477-83.8.1149, 2002.
- 882 Herceg-Bulić, I. and Kucharski, F.: North Atlantic SSTs as a Link between the Wintertime NAO and
- 883 the Following Spring Climate, *J. Clim.*, 27(1), 186–201, doi:10.1175/JCLI-D-12-00273.1, 2014.
- 884 Hersbach, H., Bell, B., Berrisford, P., Hirahara, S., Horányi, A., Muñoz-Sabater, J., Nicolas, J.,
- 885 Peubey, C., Radu, R., Schepers, D., Simmons, A., Soci, C., Abdalla, S., Abellan, X., Balsamo, G.,
- 886 Bechtold, P., Biavati, G., Bidlot, J., Bonavita, M., De Chiara, G., Dahlgren, P., Dee, D., Diamantakis,
- 887 M., Dragani, R., Flemming, J., Forbes, R., Fuentes, M., Geer, A., Haimberger, L., Healy, S., Hogan,
- 888 R. J., Hólm, E., Janisková, M., Keeley, S., Laloyaux, P., Lopez, P., Lupu, C., Radnoti, G., de Rosnay,
- 889 P., Rozum, I., Vamborg, F., Villaume, S. and Thépaut, J. N.: The ERA5 global reanalysis, *Q. J. R.*
- 890 *Meteorol. Soc.*, doi:10.1002/qj.3803, 2020.
- 891 Ionita, M., Caldarescu, D. E. and Nagavciuc, V.: Compound Hot and Dry Events in Europe:
- 892 Variability and Large-Scale Drivers, *Front. Clim.*, 3, 58, doi:10.3389/fclim.2021.688991, 2021.



893 Jesús San-Miguel-Ayanz, Tracy Durrant, Roberto Boca, Giorgio Libertà, A. B., Daniele de Rigo,  
 894 Davide Ferrari, Pieralberto Maiani, Tomàs Artés Vivancos, Duarte Oom, Hans Pfeiffer, D. and  
 895 Nuijten, T. L.: Forest Fires in Europe, Middle East and North Africa 2018., 2019.  
 896 Jones, G.: MOHC HadGEM3-GC31-LL model output prepared for CMIP6 DAMIP hist-nat, ,  
 897 doi:10.22033/ESGF/CMIP6.6059, 2019.  
 898 Kaspar, F., Müller-Westermeier, G., Penda, E., Mächel, H., Zimmermann, K., Kaiser-Weiss, A. and  
 899 Deutschländer, T.: Monitoring of climate change in Germany – data, products and services of  
 900 Germany's National Climate Data Centre, *Adv. Sci. Res.*, 10(1), 99–106, doi:10.5194/ASR-10-99-  
 901 2013, 2013.  
 902 Kautz, L.-A., Martius, O., Pfahl, S., Pinto, J. G., Ramos, A. M., Sousa, P. M. and Woollings, T.:  
 903 Atmospheric blocking and weather extremes over the Euro-Atlantic sector – a review, *Weather Clim.*  
 904 *Dyn.*, 3(1), 305–336, doi:10.5194/WCD-3-305-2022, 2022.  
 905 Kendon, M., McCarthy, M., Jevrejeva, S., Matthews, A. and Legg, T.: State of the UK climate 2018,  
 906 *Int. J. Climatol.*, 39(S1), 1–55, doi:10.1002/joc.6213, 2019.  
 907 Kennedy, J. J., Killick, R. E., Dunn, R. J., McCarthy, M. P., Morice, C. P., Rayner, N. A. and  
 908 Titchner, H. A.: Global and regional climate in 2018, *Weather*, 74(10), 332–340,  
 909 doi:10.1002/wea.3600, 2019.  
 910 Kim, H.: Global Soil Wetness Project Phase 3 Atmospheric Boundary Conditions (Experiment 1)  
 911 [Data set]. Data Integration and Analysis System (DIAS)., , doi:http://dx.doi.org/10.20783/DIAS.501,  
 912 2017.  
 913 Kohonen, T.: Essentials of the self-organizing map, *Neural Networks*, 37, 52–65,  
 914 doi:10.1016/j.neunet.2012.09.018, 2013.  
 915 Lange, S.: Trend-preserving bias adjustment and statistical downscaling with ISIMIP3BASD (v1.0),  
 916 *Geosci. Model Dev.*, 12(7), 3055–3070, doi:10.5194/GMD-12-3055-2019, 2019.  
 917 Leach, N. J., Li, S., Sparrow, S., Oldenborgh, G. J. van, Lott, F. C., Weisheimer, A. and Allen, M. R.:  
 918 Anthropogenic Influence on the 2018 Summer Warm Spell in Europe: The Impact of Different  
 919 Spatio-Temporal Scales, *Bull. Am. Meteorol. Soc.*, 101(1), S41–S46, doi:10.1175/BAMS-D-19-  
 920 0201.1, 2020.  
 921 Li, M., Yao, Y., Simmonds, I., Luo, D., Zhong, L. and Chen, X.: Collaborative impact of the nao and  
 922 atmospheric blocking on european heatwaves, with a focus on the hot summer of 2018, *Environ. Res.*  
 923 *Lett.*, 15(11), 114003, doi:10.1088/1748-9326/aba6ad, 2020.  
 924 Liu, X., He, B., Guo, L., Huang, L. and Chen, D.: Similarities and Differences in the Mechanisms  
 925 Causing the European Summer Heatwaves in 2003, 2010, and 2018, *Earth's Futur.*, 8(4),  
 926 e2019EF001386, doi:10.1029/2019EF001386, 2020.  
 927 Lo, M. H., Wu, W. Y., Tang, L. I., Ryu, D., Rashid, M. and Wu, R. J.: Temporal Changes in Land  
 928 Surface Coupling Strength: An Example in a Semi-Arid Region of Australia, *J. Clim.*, 34(4), 1503–  
 929 1513, doi:10.1175/JCLI-D-20-0250.1, 2021.  
 930 Lutz, F., Herzfeld, T., Heinke, J., Rolinski, S., Schaphoff, S., Von Bloh, W., Stoorvogel, J. J. and  
 931 Müller, C.: Simulating the effect of tillage practices with the global ecosystem model LPJmL (version  
 932 5.0-tillage), *Geosci. Model Dev.*, 12(6), 2419–2440, doi:10.5194/GMD-12-2419-2019, 2019.  
 933 Maher, N., Milinski, S., Suarez-Gutierrez, L., Botzet, M., Dobrynin, M., Kornblueh, L., Kröger, J.,  
 934 Takano, Y., Ghosh, R., Hedemann, C., Li, C., Li, H., Manzini, E., Notz, D., Putrasahan, D., Boysen,  
 935 L., Claussen, M., Ilyina, T., Olonscheck, D., Raddatz, T., Stevens, B. and Marotzke, J.: The Max  
 936 Planck Institute Grand Ensemble: Enabling the Exploration of Climate System Variability, *J. Adv.*  
 937 *Model. Earth Syst.*, 11(7), 2050–2069, doi:10.1029/2019MS001639, 2019.  
 938 Manning, C., Widmann, M., Bevacqua, E., Van Loon, A. F., Maraun, D. and Vrac, M.: Increased  
 939 probability of compound long-duration dry and hot events in Europe during summer (1950–2013),  
 940 *Environ. Res. Lett.*, 14(9), 094006, doi:10.1088/1748-9326/AB23BF, 2019.  
 941 Markonis, Y., Kumar, R., Hanel, M., Rakovec, O., Máca, P. and Kouchak, A. A.: The rise of  
 942 compound warm-season droughts in Europe, *Sci. Adv.*, 7(6),  
 943 doi:10.1126/SCIADV.ABB9668/SUPPL\_FILE/ABB9668\_SM.PDF, 2021.  
 944 Masson-Delmotte, V., P. Zhai, A. Pirani, S. L., Connors, C. Péan, S. Berger, N. Caud, Y. Chen, L.  
 945 Goldfarb, M. I. Gomis, M. Huang, K. Leitzell, E. Lonnoy, J. B. R. and Matthews, T. K. Maycock, T.  
 946 Waterfield, O. Yelekçi, R. Yu, and B. Z. (eds. : IPCC, 2021: Climate Change 2021: The Physical  
 947 Science Basis. Contribution of Working Group I to the Sixth Assessment Report of the



- 948 Intergovernmental Panel on Climate Change, New York., 2021.
- 949 McCarthy, M., Christidis, N., Dunstone, N., Fereday, D., Kay, G., Klein-Tank, A., Lowe, J., Petch, J.,
- 950 Scaife, A. and Stott, P.: Drivers of the UK summer heatwave of 2018, *Weather*, 74(11), 390–396,
- 951 doi:10.1002/WEA.3628, 2019.
- 952 Mckee, T. B., Doesken, N. J. and Kleist, J.: THE RELATIONSHIP OF DROUGHT FREQUENCY
- 953 AND DURATION TO TIME SCALES, Eighth Conf. Appl. Climatol., 17–22, 1993.
- 954 Miralles, D. G., Teuling, A. J., van Heerwaarden, C. C. and Vilà-Guerau de Arellano, J.: Mega-
- 955 heatwave temperatures due to combined soil desiccation and atmospheric heat accumulation, *Nat.*
- 956 *Geosci.*, 7(5), 345–349, doi:10.1038/ngeo2141, 2014.
- 957 Di Napoli, C., Barnard, C., Prudhomme, C., Cloke, H. L. and Pappenberger, F.: ERA5-HEAT: A
- 958 global gridded historical dataset of human thermal comfort indices from climate reanalysis, *Geosci.*
- 959 *Data J.*, 8(1), 2–10, doi:10.1002/gdj3.102, 2021.
- 960 Orth, R.: When the Land Surface Shifts Gears, *AGU Adv.*, 2(2), e2021AV000414,
- 961 doi:10.1029/2021av000414, 2021.
- 962 Ossó, A., Sutton, R., Shaffrey, L. and Dong, B.: Development, Amplification, and Decay of
- 963 Atlantic/European Summer Weather Patterns Linked to Spring North Atlantic Sea Surface
- 964 Temperatures, *J. Clim.*, 33(14), 5939–5951, doi:10.1175/JCLI-D-19-0613.1, 2020.
- 965 Pascal, M., Lagarrigue, R., Tabai, A., Bonmarin, I., Camail, S., Laaidi, K., Le Tertre, A. and Denys,
- 966 S.: Evolving heat waves characteristics challenge heat warning systems and prevention plans, *Int. J.*
- 967 *Biometeorol.*, 65(10), 1683–1694, doi:10.1007/S00484-021-02123-Y/FIGURES/5, 2021.
- 968 Perkins-Kirkpatrick, S. E. and Lewis, S. C.: Increasing trends in regional heatwaves, *Nat. Commun.*,
- 969 11(1), 3357, doi:10.1038/s41467-020-16970-7, 2020.
- 970 Peters, W., Bastos, A., Ciais, P. and Vermeulen, A.: A historical, geographical and ecological
- 971 perspective on the 2018 European summer drought, *Philos. Trans. R. Soc. B*, 375(1810),
- 972 doi:10.1098/RSTB.2019.0505, 2020.
- 973 Philip, S., Kew, S., van Oldenborgh, G. J., Otto, F., Vautard, R., van der Wiel, K., King, A., Lott, F.,
- 974 Arrighi, J., Singh, R. and van Aalst, M.: A protocol for probabilistic extreme event attribution
- 975 analyses, *Adv. Stat. Climatol. Meteorol. Oceanogr.*, 6(2), 177–203, doi:10.5194/ascmo-6-177-2020,
- 976 2020.
- 977 Philip, S. Y., Kew, S. F., Oldenborgh, G. J. Van, Yang, W., Vecchi, G. A., Anslow, F. S., Li, S.,
- 978 Seneviratne, S. I., Luu, L. N., Arrighi, J., Singh, R., Aalst, V., Hauser, M., Schumacher, D. L.,
- 979 Marghidan, C. P., Ebi, K. L., Vautard, R., Tradowsky, J., Coumou, D., Lehner, F., Rodell, C., Stull,
- 980 R., Howard, R., Gillett, N. and Otto, F. E. L.: Rapid attribution analysis of the extraordinary heatwave
- 981 on the Pacific Coast of the US and Canada June 2021, *Earth Syst. Dyn. Discuss.*, in review [online]
- 982 Available from: [https://www.worldweatherattribution.org/wp-content/uploads/NW-US-extreme-heat-](https://www.worldweatherattribution.org/wp-content/uploads/NW-US-extreme-heat-2021-scientific-report-WWA.pdf)
- 983 [2021-scientific-report-WWA.pdf](https://www.worldweatherattribution.org/wp-content/uploads/NW-US-extreme-heat-2021-scientific-report-WWA.pdf), 2021.
- 984 Prodhomme, C., Materia, S., Ardilouze, C., White, R. H., Batté, L., Guemas, V., Fragkoulidis, G. and
- 985 García-Serrano, J.: Seasonal prediction of European summer heatwaves, *Clim. Dyn.*, 1, 3,
- 986 doi:10.1007/s00382-021-05828-3, 2021.
- 987 Quesada, B., Vautard, R., Yiou, P., Hirschi, M. and Seneviratne, S. I.: Asymmetric European summer
- 988 heat predictability from wet and dry southern winters and springs, *Nat. Clim. Chang.* 2012 210, 2(10),
- 989 736–741, doi:10.1038/nclimate1536, 2012.
- 990 Ridley, J., Menary, M., Kuhlbrodt, T., Andrews, M. and Andrews, T.: MOHC HadGEM3-GC31-LL
- 991 model output prepared for CMIP6 CMIP historical, , doi:10.22033/ESGF/CMIP6.6109, 2019.
- 992 Rousi, E., Anagnostopoulou, C., Tolika, K. and Maheras, P.: Representing teleconnection patterns
- 993 over Europe: A comparison of SOM and PCA methods, *Atmos. Res.*, 152, 123–137,
- 994 doi:10.1016/j.atmosres.2013.11.010, 2015.
- 995 Rousi, E., Selten, F., Rahmstorf, S. and Coumou, D.: Changes in North Atlantic Atmospheric
- 996 Circulation in a Warmer Climate Favor Winter Flooding and Summer Drought over Europe, *J. Clim.*,
- 997 34(6), 2277–2295, doi:10.1175/JCLI-D-20-0311.1, 2021.
- 998 Rousi, E., Kornhuber, K., Beobide-Arsuaga, G., Luo, F. and Coumou, D.: Accelerated western
- 999 European heatwave trends linked to more-persistent double jets over Eurasia, *Nat. Commun.* 2022
- 1000 131, 13(1), 1–11, doi:10.1038/s41467-022-31432-y, 2022.
- 1001 Russo, S., Dosio, A., Graversen, R. G., Sillmann, J., Carrao, H., Dunbar, M. B., Singleton, A.,
- 1002 Montagna, P., Barbola, P. and Vogt, J. V.: Magnitude of extreme heat waves in present climate and





- 1003 their projection in a warming world, *J. Geophys. Res. Atmos.*, 119(22), 12,500–12,512,
- 1004 doi:10.1002/2014JD022098, 2014.
- 1005 Russo, S., Sillmann, J. and Fischer, E. M.: Top ten European heatwaves since 1950 and their
- 1006 occurrence in the coming decades, *Environ. Res. Lett.*, 10(12), 124003, doi:10.1088/1748-
- 1007 9326/10/12/124003, 2015.
- 1008 Saeed, S., Van Lipzig, N., Müller, W. A., Saeed, F. and Zanchettin, D.: Influence of the circumglobal
- 1009 wave-train on European summer precipitation, *Clim. Dyn.* 2013 431, 43(1), 503–515,
- 1010 doi:10.1007/S00382-013-1871-0, 2013.
- 1011 Santos, J. A., Pfahl, S., Pinto, J. G. and Wernli, H.: Mechanisms underlying temperature extremes in
- 1012 Iberia: a Lagrangian perspective, *New pub Stock. uni Press*, 67(1), 1–15,
- 1013 doi:10.3402/TELLUSA.V67.26032, 2015.
- 1014 Schädler, G. and Breil, M.: Identification of droughts and heatwaves in Germany with regional
- 1015 climate networks, *Nonlinear Process. Geophys.*, 28(2), 231–245, doi:10.5194/npg-28-231-2021, 2021.
- 1016 Schaphoff, S., Von Bloh, W., Rammig, A., Thonicke, K., Biemans, H., Forkel, M., Gerten, D.,
- 1017 Heinke, J., Jägermeyr, J., Knauer, J., Langerwisch, F., Lucht, W., Müller, C., Rolinski, S. and Waha,
- 1018 K.: LPJmL4 - A dynamic global vegetation model with managed land - Part 1: Model description,
- 1019 *Geosci. Model Dev.*, 11(4), 1343–1375, doi:10.5194/GMD-11-1343-2018, 2018.
- 1020 Scherrer, S. C., Croci-Maspoli, M., Schwierz, C. and Appenzeller, C.: Two-dimensional indices of
- 1021 atmospheric blocking and their statistical relationship with winter climate patterns in the Euro-
- 1022 Atlantic region, *Int. J. Climatol.*, 26(2), 233–249, doi:10.1002/JOC.1250, 2006.
- 1023 Schuldt, B., Buras, A., Arend, M., Vitasse, Y., Beierkuhnlein, C., Damm, A., Gharun, M., Grams, T.
- 1024 E. E., Hauck, M., Hajek, P., Hartmann, H., Hiltbrunner, E., Hoch, G., Holloway-Phillips, M., Körner,
- 1025 C., Larysch, E., Lübke, T., Nelson, D. B., Rammig, A., Rigling, A., Rose, L., Ruehr, N. K.,
- 1026 Schumann, K., Weiser, F., Werner, C., Wohlgemuth, T., Zang, C. S. and Kahmen, A.: A first
- 1027 assessment of the impact of the extreme 2018 summer drought on Central European forests, *Basic*
- 1028 *Appl. Ecol.*, 45, 86–103, doi:10.1016/J.BAAE.2020.04.003, 2020.
- 1029 Schuster, M., Grieger, J., Richling, A., Schartner, T., Illing, S., Kadow, C., Müller, W. A., Pohlmann,
- 1030 H., Pfahl, S. and Ulbrich, U.: Improvement in the decadal prediction skill of the North Atlantic
- 1031 extratropical winter circulation through increased model resolution, *Earth Syst. Dyn.*, 10(4), 901–917,
- 1032 doi:10.5194/ESD-10-901-2019, 2019.
- 1033 Seneviratne, S. I., Corti, T., Davin, E. L., Hirschi, M., Jaeger, E. B., Lehner, I., Orlowsky, B. and
- 1034 Teuling, A. J.: Investigating soil moisture–climate interactions in a changing climate: A review,
- 1035 *Earth-Science Rev.*, 99(3), 125–161, doi:https://doi.org/10.1016/j.earscirev.2010.02.004, 2010.
- 1036 Senf, C. and Seidl, R.: Persistent impacts of the 2018 drought on forest disturbance regimes in
- 1037 Europe, *Biogeosciences*, 18(18), 5223–5230, doi:10.5194/BG-18-5223-2021, 2021.
- 1038 Shepherd, T. G.: A Common Framework for Approaches to Extreme Event Attribution, *Curr. Clim.*
- 1039 *Chang. Reports*, 2(1), 28–38, doi:10.1007/S40641-016-0033-Y/FIGURES/7, 2016.
- 1040 Shiogama, H.: MIROC MIROC6 model output prepared for CMIP6 DAMIP hist-nat, ,
- 1041 doi:10.22033/ESGF/CMIP6.5583, 2019.
- 1042 Sinclair, V. A., Mikkola, J., Rantanen, M. and Räisänen, J.: The summer 2018 heatwave in Finland,
- 1043 *Weather*, 74(11), 403–409, doi:10.1002/WEA.3525, 2019.
- 1044 Sousa, P. M., Trigo, R. M., Barriopedro, D., Soares, P. M. M., Ramos, A. M. and Liberato, M. L. R.:  
Responses of European precipitation distributions and regimes to different blocking locations, *Clim.*
- 1045 *Dyn.*, 48(3–4), 1141–1160, doi:10.1007/S00382-016-3132-5/FIGURES/12, 2017.
- 1046 Sousa, P. M., Trigo, R. M., Barriopedro, D., Soares, P. M. M. and Santos, J. A.: European temperature
- 1047 responses to blocking and ridge regional patterns, *Clim. Dyn.*, 50(1–2), 457–477,
- 1048 doi:10.1007/s00382-017-3620-2, 2018.
- 1049 Sousa, P. M., Barriopedro, D., Ramos, A. M., García-Herrera, R., Espírito-Santo, F. and Trigo, R. M.:  
Saharan air intrusions as a relevant mechanism for Iberian heatwaves: The record breaking events of
- 1050 August 2018 and June 2019, *Weather Clim. Extrem.*, 26, 100224, doi:10.1016/j.wace.2019.100224,
- 1051 2019.
- 1052 Spensberger, C., Madonna, E., Boettcher, M., Grams, C. M., Papritz, L., Quinting, J. F.,
- 1053 Röthlisberger, M., Sprenger, M. and Zschenderlein, P.: Dynamics of concurrent and sequential
- 1054 Central European and Scandinavian heatwaves, *Q. J. R. Meteorol. Soc.*, 146(732), 2998–3013,
- 1055 doi:10.1002/qj.3822, 2020.
- 1056
- 1057



- 1058 Spinoni, J., Vogt, J. V., Naumann, G., Barbosa, P. and Dosio, A.: Will drought events become more  
1059 frequent and severe in Europe?, *Int. J. Climatol.*, 38(4), 1718–1736, doi:10.1002/JOC.5291, 2018.
- 1060 Spinoni, J., Barbosa, P., Buchignani, E., Cassano, J., Cavazos, T., Christensen, J. H., Christensen, O.  
1061 B., Coppola, E., Evans, J., Geyer, B., Giorgi, F., Hadjinicolaou, P., Jacob, D., Katzfey, J., Koenigk,  
1062 T., Laprise, R., Lennard, C. J., Kurnaz, M. L., Delei, L. I., Llopart, M., McCormick, N., Naumann, G.,  
1063 Nikulin, G., Ozturk, T., Panitz, H. J., da Rocha, R. P., Rockel, B., Solman, S. A., Syktus, J., Tangang,  
1064 F., Teichmann, C., Vautard, R., Vogt, J. V., Winger, K., Zittis, G. and Dosio, A.: Future global  
1065 meteorological drought hot spots: A study based on CORDEX data, *J. Clim.*, 33(9), 3635–3661,  
1066 doi:10.1175/JCLI-D-19-0084.1, 2020.
- 1067 Sprenger, M. and Wernli, H.: The LAGRANTO Lagrangian analysis tool - Version 2.0, *Geosci.*  
1068 *Model Dev.*, 8(8), 2569–2586, doi:10.5194/GMD-8-2569-2015, 2015.
- 1069 Stott, P. A., Stone, D. A. and Allen, M. R.: Human contribution to the European heatwave of 2003,  
1070 *Nature*, 432(7017), 610–614, doi:10.1038/nature03089, 2004.
- 1071 Suarez-Gutierrez, L., Li, C., Müller, W. A. and Marotzke, J.: Internal variability in European summer  
1072 temperatures at 1.5 °C and 2 °C of global warming, *Environ. Res. Lett.*, 13(6), 064026,  
1073 doi:10.1088/1748-9326/AABA58, 2018.
- 1074 Suarez-Gutierrez, L., Milinski, S. and Maher, N.: Exploiting large ensembles for a better yet simpler  
1075 climate model evaluation, *Clim. Dyn.*, 57(9–10), 2557–2580, doi:10.1007/S00382-021-05821-  
1076 W/FIGURES/8, 2021.
- 1077 Swart, N. C., Cole, J. N. S., Kharin, V. V., Lazare, M., Scinocca, J. F., Gillett, N. P., Anstey, J., Arora,  
1078 V., Christian, J. R., Jiao, Y., Lee, W. G., Majaess, F., Saenko, O. A., Seiler, C., Seinen, C., Shao, A.,  
1079 Solheim, L., von Salzen, K., Yang, D., Winter, B. and Sigmond, M.: CCCma CanESM5 model output  
1080 prepared for CMIP6 CMIP historical, , doi:10.22033/ESGF/CMIP6.3610, 2019a.
- 1081 Swart, N. C., Cole, J. N. S., Kharin, V. V., Lazare, M., Scinocca, J. F., Gillett, N. P., Anstey, J., Arora,  
1082 V., Christian, J. R., Jiao, Y., Lee, W. G., Majaess, F., Saenko, O. A., Seiler, C., Seinen, C., Shao, A.,  
1083 Solheim, L., von Salzen, K., Yang, D., Winter, B. and Sigmond, M.: CCCma CanESM5 model output  
1084 prepared for CMIP6 DAMIP hist-nat, , doi:10.22033/ESGF/CMIP6.3601, 2019b.
- 1085 Tatebe, H. and Watanabe, M.: MIROC MIROC6 model output prepared for CMIP6 CMIP historical, ,  
1086 doi:10.22033/ESGF/CMIP6.5603, 2018.
- 1087 Toreti, A., Belward, A., Perez-Dominguez, I., Naumann, G., Luterbacher, J., Cronie, O., Seguini, L.,  
1088 Manfron, G., Lopez-Lozano, R., Baruth, B., van den Berg, M., Dentener, F., Ceglar, A.,  
1089 Chatzopoulos, T. and Zampieri, M.: The Exceptional 2018 European Water Seesaw Calls for Action  
1090 on Adaptation, *Earth's Futur.*, 7(6), 652–663, doi:10.1029/2019EF001170, 2019.
- 1091 Tradowsky, J. S., Bird, L., Kreft, P. V., Rosier, S. M., Soltanzadeh, I., Stone, D. A. and Bodeker, G.  
1092 E.: Toward Near-Real-Time Attribution of Extreme Weather Events in Aotearoa New Zealand, *Bull.*  
1093 *Am. Meteorol. Soc.*, 103(3), S105–S110, doi:10.1175/BAMS-D-21-0236.1, 2022.
- 1094 Tsonis, A. A., Swanson, K. L. and Roebber, P. J.: What Do Networks Have to Do with Climate?,  
1095 *Bull. Am. Meteorol. Soc.*, 87(5), 585–596, doi:10.1175/BAMS-87-5-585, 2006.
- 1096 Vicente-Serrano, S. M., Azorin-Molina, C., Sanchez-Lorenzo, A., Revuelto, J., Morán-Tejeda, E.,  
1097 López-Moreno, J. I. and Espejo, F.: Sensitivity of reference evapotranspiration to changes in  
1098 meteorological parameters in Spain (1961–2011), *Water Resour. Res.*, 50(11), 8458–8480,  
1099 doi:10.1002/2014WR015427, 2014.
- 1100 Vogel, M. M., Zscheischler, J., Wartenburger, R., Dee, D. and Seneviratne, S. I.: Concurrent 2018  
1101 Hot Extremes Across Northern Hemisphere Due to Human-Induced Climate Change, *Earth's Futur.*,  
1102 7(7), 692–703, doi:10.1029/2019EF001189, 2019.
- 1103 Voldoire, A.: CMIP6 simulations of the CNRM-CERFACS based on CNRM-CM6-1 model for CMIP  
1104 experiment historical, , doi:10.22033/ESGF/CMIP6.4066, 2018.
- 1105 Voldoire, A.: CNRM-CERFACS CNRM-CM6-1 model output prepared for CMIP6 DAMIP hist-nat,  
1106 , doi:10.22033/ESGF/CMIP6.4048, 2019.
- 1107 Wehrli, K., Guillod, B. P., Hauser, M., Leclair, M. and Seneviratne, S. I.: Identifying Key Driving  
1108 Processes of Major Recent Heat Waves, *J. Geophys. Res. Atmos.*, 124(22), 11746–11765,  
1109 doi:10.1029/2019JD030635, 2019.
- 1110 Wehrli, K., Hauser, M. and Seneviratne, S. I.: Storylines of the 2018 Northern Hemisphere heatwave  
1111 at pre-industrial and higher global warming levels, *Earth Syst. Dyn.*, 11(4), 855–873,  
1112 doi:10.5194/ESD-11-855-2020, 2020.





- 1113 Woollings, T., Pinto, J. G. and Santos, J. A.: Dynamical Evolution of North Atlantic Ridges and  
 1114 Poleward Jet Stream Displacements, *J. Atmos. Sci.*, 68(5), 954–963, doi:10.1175/2011JAS3661.1,  
 1115 2011.
- 1116 Woollings, T., Barriopedro, D., Methven, J., Son, S. W., Martius, O., Harvey, B., Sillmann, J., Lupo,  
 1117 A. R. and Seneviratne, S.: Blocking and its Response to Climate Change, *Curr. Clim. Chang. Reports*,  
 1118 4(3), 287–300, doi:10.1007/s40641-018-0108-z, 2018.
- 1119 World Weather Attribution (WWA): Heatwave in northern Europe, summer 2018, [online] Available  
 1120 from: <https://www.worldweatherattribution.org/attribution-of-the-2018-heat-in-northern-europe/>  
 1121 (Accessed 18 August 2022), 2018.
- 1122 World Weather Attribution (WWA): Without human-caused climate change temperatures of 40°C in  
 1123 the UK would have been extremely unlikely, [online] Available from:  
 1124 [https://www.worldweatherattribution.org/without-human-caused-climate-change-temperatures-of-](https://www.worldweatherattribution.org/without-human-caused-climate-change-temperatures-of-40c-in-the-uk-would-have-been-extremely-unlikely/)  
 1125 [40c-in-the-uk-would-have-been-extremely-unlikely/](https://www.worldweatherattribution.org/without-human-caused-climate-change-temperatures-of-40c-in-the-uk-would-have-been-extremely-unlikely/) (Accessed 18 August 2022), 2022.
- 1126 Yukimoto, S., Koshiro, T., Kawai, H., Oshima, N., Yoshida, K., Urakawa, S., Tsujino, H., Deushi,  
 1127 M., Tanaka, T., Hosaka, M., Yoshimura, H., Shindo, E., Mizuta, R., Ishii, M., Obata, A. and Adachi,  
 1128 Y.: MRI MRI-ESM2.0 model output prepared for CMIP6 CMIP historical, ,  
 1129 doi:10.22033/ESGF/CMIP6.6842, 2019a.
- 1130 Yukimoto, S., Koshiro, T., Kawai, H., Oshima, N., Yoshida, K., Urakawa, S., Tsujino, H., Deushi,  
 1131 M., Tanaka, T., Hosaka, M., Yoshimura, H., Shindo, E., Mizuta, R., Ishii, M., Obata, A. and Adachi,  
 1132 Y.: MRI MRI-ESM2.0 model output prepared for CMIP6 DAMIP hist-nat, ,  
 1133 doi:10.22033/ESGF/CMIP6.6825, 2019b.
- 1134 Zampieri, M., Ceglar, A., Dentener, F. and Toreti, A.: Wheat yield loss attributable to heat waves,  
 1135 drought and water excess at the global, national and subnational scales, *Environ. Res. Lett.*, 12(6),  
 1136 064008, doi:10.1088/1748-9326/AA723B, 2017.
- 1137 Ziehn, T., Chamberlain, M., Lenton, A., Law, R., Bodman, R., Dix, M., Wang, Y., Dobrohotoff, P.,  
 1138 Srbinovsky, J., Stevens, L., Vohralik, P., Mackallah, C., Sullivan, A., O’Farrell, S. and Druken, K.:  
 1139 CSIRO ACCESS-ESM1.5 model output prepared for CMIP6 CMIP historical, ,  
 1140 doi:10.22033/ESGF/CMIP6.4272, 2019.
- 1141 Ziehn, T., Dix, M., Mackallah, C., Chamberlain, M., Lenton, A., Law, R., Druken, K. and Ridzwan,  
 1142 S. M.: CSIRO ACCESS-ESM1.5 model output prepared for CMIP6 DAMIP hist-nat, ,  
 1143 doi:10.22033/ESGF/CMIP6.14378, 2020.
- 1144 Zscheischler, J. and Fischer, E. M.: The record-breaking compound hot and dry 2018 growing season  
 1145 in Germany, *Weather Clim. Extrem.*, 29, 100270, doi:10.1016/j.wace.2020.100270, 2020.
- 1146 Zscheischler, J., Martius, O., Westra, S., Bevacqua, E., Raymond, C., Horton, R. M., van den Hurk,  
 1147 B., AghaKouchak, A., Jézéquel, A., Mahecha, M. D., Maraun, D., Ramos, A. M., Ridder, N. N.,  
 1148 Thiery, W. and Vignotto, E.: A typology of compound weather and climate events, *Nat. Rev. Earth*  
 1149 *Environ.*, 1(7), 333–347, doi:10.1038/s43017-020-0060-z, 2020.
- 1150 Zschenderlein, P., Pfahl, S., Wernli, H. and Fink, A. H.: A Lagrangian analysis of upper-tropospheric  
 1151 anticyclones associated with heat waves in Europe, *Weather Clim. Dyn.*, 1(1), 191–206,  
 1152 doi:10.5194/wcd-1-191-2020, 2020.